Received: 28 May 2021 | Revised: 24 November 2021 | Accepted: 30 November 2021

DOI: 10.1111/mmi.14853

RESEARCH ARTICLE

WILEY

Contribution of a ZIP-family protein to manganese uptake and infective endocarditis virulence in *Streptococcus sanguinis*

Tanya Puccio | **Karina S. Kunka** | **Seon-Sook An** | **Todd Kitten**

Philips Institute for Oral Health Research, Virginia Commonwealth University School of Dentistry, Richmond, Virginia, USA

Correspondence
Todd Kitten, Philips Institute for Oral Health Research, Virginia Commonwealth University School of Dentistry, Richmond, VA, USA.
Email: tkitten@vcu.edu

Funding information
This work was supported by the National Institutes of Health: award F31 DE028468 to TP from the National Institute of Dental and Craniofacial Research and award R01 AI114926 to TK from the National Institute of Allergy and Infectious Diseases. The content is solely the responsibility of the authors and does not necessarily represent the official views of the National Institutes of Health.

Abstract

Streptococcus sanguinis is an important cause of infective endocarditis. In strain SK36, the ABC-family manganese transporter, SsaACB, is essential for virulence. We have now identified a ZIP-family protein, TmpA, as a secondary manganese transporter. A *tmpA* mutant had no phenotype, but a Δ*ssaACB* Δ*tmpA* mutant was more attenuated for serum growth and for virulence in a rabbit model than its Δ*ssaACB* parent. The growth of both mutants was restored by supplemental manganese, but the Δ*ssaACB* Δ*tmpA* mutant required twenty-fold more and accumulated less. Although ZIP-family proteins are known for zinc and iron transport, TmpA-mediated transport of either metal was minimal. While *ssaACB* appears ubiquitous in *St. sanguinis*, *tmpA* was present in a majority of strains and a *mntH* gene encoding an NRAMP-family transporter was identified in relatively few, including VMC66. As in SK36, deletion of *ssaACB* greatly diminished VMC66 endocarditis virulence and serum growth, and deletion of *tmpA* from this mutant diminished virulence further. Virulence was not significantly altered by deletion of *mntH* from either VMC66 or its Δ*ssaACB* mutant. This and the accompanying paper together suggest that SsaACB is of primary importance for endocarditis virulence while secondary transporters TmpA and MntH contribute to growth under differing conditions.

KEYWORDS
bacterial endocarditis, manganese transport, membrane protein, rabbit model, ZIP-family protein

1 | INTRODUCTION

Infective endocarditis (IE) is a disease caused by microorganisms entering the bloodstream and colonizing damaged heart valves, leading to potentially fatal complications such as congestive heart failure, aneurysm, and stroke (Bashore et al., 2006). Many recent studies suggest that IE incidence is rising (Quan et al., 2020), and mortality rates of 12%–30% are common (Jamil et al., 2019; Ly et al., 2020). Currently, prevention is limited to prophylactic antibiotics before dental procedures (Wilson et al., 2021). The economic burden, potential for side effects, and questionable efficacy (Dayer & Thornhill, 2018; Quan et al., 2020; Thornhill et al., 2018) of this practice, as well as the increasing prevalence of antibiotic resistance (Dodds, 2017), suggest the need for new approaches to prevention. In addition, the ability of oral bacteria to enter the bloodstream through any opening in the oral mucosa, which may occur during routine hygiene practices or mastication (Wilson et al., 2007; Wray et al., 2008), explains why prophylaxis given before dental procedures can never prevent all IE. Thus, it would be desirable to identify a drug target that is specific to endocarditis pathogenesis, which

would allow future prophylactic drugs to be taken on a daily basis without disturbing the microbiome or selecting for resistance.

Streptococcus sanguinis is one of the most common oral bacteria to be isolated from IE patients (Di Filippo et al., 2006). It is typically considered a commensal in the oral cavity due to an antagonistic relationship with the caries pathogen *Streptococcus mutans* (Kreth et al., 2005). The trace element manganese (Mn) plays a role in the virulence of *St. sanguinis* (Crump et al., 2014; Das et al., 2009) as well as other streptococci (Eijkelkamp et al., 2015) and bacterial pathogens (Juttukonda & Skaar, 2015; Kelliher & Kehl-Fie, 2016). Manganese import in bacteria has been confirmed in at least two protein families: ATP-binding cassettes (ABC) and natural resistance-associated macrophage proteins (NRAMP) (Waters, 2020). A knockout mutant of the lipoprotein component of an ABC manganese transporter in *St. sanguinis*, SsaB, is deficient in manganese transport as well as in aerobic serum growth (Crump et al., 2014). This growth defect was rescued by the addition of only 2 μM Mn^{2+}, indicating that manganese is able to enter *St. sanguinis* cells despite the absence of the primary transporter. The genome annotation of *St. sanguinis* SK36 (Xu et al., 2007) did not indicate the presence of any additional canonical manganese transporters, which led us to examine other metal transport protein families. NRAMP-family proteins (Nevo & Nelson, 2006) are encoded by at least eight *St. sanguinis* strains but not by SK36. These proteins, often named MntH, have been found to contribute to manganese uptake and acid tolerance in other streptococci (Kajfasz et al., 2020; Shabayek et al., 2016).

The family of ZRT-, IRT-like proteins (ZIP) is well-known for its role in the transport of zinc (Zn), iron (Fe), or other metals across cellular membranes (Eide, 2004). The ZIP family takes its name from the first identified members: zinc regulated transporters (ZRT1 and ZRT2) found in *Saccharomyces cerevisiae* (Zhao & Eide, 1996a, 1996b) and iron-regulated transporter (IRT1) from *Arabidopsis thaliana* (Eide et al., 1996). Since these initial discoveries, ZIP-family proteins have been identified in organisms of various phyla, including 14 in humans (Jeong & Eide, 2013). While ZIP-family proteins principally transport zinc or iron, two human versions, hZIP8 (Fujishiro & Himeno, 2019; Park et al., 2015) and hZIP14 (Aydemir et al., 2017; Scheiber et al., 2019), as well as BmtA from *Borreliella burgdorferi* (Ouyang et al., 2009; Ramsey et al., 2017) primarily transport manganese. Bacterial ZIP proteins fall into the GufA subfamily (Gaither & Eide, 2001), which also contains mammalian members such as hZIP11 (Dempski, 2012; Yu et al., 2013). The first bacterial ZIP protein, ZupT, was identified in *Escherichia coli* (Grass et al., 2002). This initial study proved that it played a role in zinc uptake, and further investigation determined that other metal cations could also be transported by ZupT, albeit with lower affinity (Grass et al., 2005; Taudte & Grass, 2010). Many bacterial species contain putative ZIP-family proteins, but few have been characterized for metal specificity or contribution to growth and virulence.

Here we confirm that ZIP-family proteins should be considered an additional family of bacterial manganese importers. We report that a ZIP-family protein in *St. sanguinis* contributes to manganese uptake in an Δ*ssaACB* mutant, which is deleted for the ABC-family manganese transporter, and we establish its contribution to IE virulence. We extended this study to additional *St. sanguinis* strains, including two that encode MntH homologs. To our knowledge, we have performed the most extensive analysis of the role of distinct protein families in manganese uptake and virulence that has ever been performed in any *Streptococcus*.

2 | RESULTS

2.1 | Identification of a ZIP-family protein

Given the low concentration of manganese required to rescue the growth of the Δ*ssaB* mutant (Crump et al., 2014), we hypothesized that there was a secondary manganese transporter encoded by the *St. sanguinis* SK36 genome. Previously, studies in *B. burgdorferi* reported that a ZIP-family protein, BmtA, transported primarily manganese instead of zinc or iron (Ouyang et al., 2009; Ramsey et al., 2017). Since the discovery and characterization of ZupT in *Ec. coli* (Grass et al., 2002), few bacterial ZIP-family proteins have been characterized for their metal selectivity and only two have been found to contribute to virulence: BmtA (Ouyang et al., 2009) and ZupT in *Clostridioides difficile* (Zackular et al., 2020). *C. difficile* ZupT, like most ZIP-family proteins, was found to principally transport zinc. When examining the genome of SK36, we identified SSA_1413 (SSA_RS06930) as a ZIP-family protein based on comparison to the sequence of BmtA.

2.2 | Deletion of the ZIP-family protein gene results in manganese deficiency in an Δ*ssaACB* background

To determine the function of SSA_1413, the knockout strain from an *St. sanguinis* SK36 mutant library (Xu et al., 2011) was utilized. The kanamycin (Kan) resistance cassette and flanking region from the SSX_1413 strain were amplified and transformed into a tetracycline (Tet) resistant Δ*ssaACB* single transport system mutant in an attempt to create a Δ*ssaACB* ΔSSA_1413 double mutant. Initial attempts to introduce the ΔSSA_1413 mutation into the Δ*ssaACB* background were unsuccessful (data not shown). This was not due to lack of competence, as we have previously generated mutants in this strain (Murgas et al., 2020; Puccio et al., 2020). Additionally, this same DNA construct was used to generate the ΔSSA_1413 strain in SK36. Transformants in the Δ*ssaACB* background were obtained only when the brain heart infusion (BHI) agar plates were supplemented with 10 μM Mn^{2+}. While the single mutant grew similar to wild type (WT) in BHI media, the double mutant required 10 μM Mn^{2+} supplementation to grow to WT levels overnight (data not shown). Because of these results and others described below, we concluded that SSA_1413 is a metal transporter, which we have named TmpA for transport of metal protein A. This name was also chosen to avoid species- and metal-specific nomenclature.

Serum contains nanomolar concentrations of manganese (Murgas et al., 2020) and the oxygen concentration of arterial blood is 12% (Atkuri et al., 2007). In these conditions, growth of WT and Δ*ssaB* mutant strains was determined to be analogous to that observed in our rabbit model of IE, which entails infection of the aortic valve (Crump et al., 2014). At this O_2 concentration, deletion of *tmpA* from the WT and Δ*ssaACB* backgrounds led to only slight, non-significant differences in growth (Figure 1a). When the O_2 concentration was reduced to 6% or 1%, growth of the double mutant at 24 hr was significantly less than the Δ*ssaACB* parent strain (Figure 1a). In contrast, growth of the single mutant was not statistically different from WT under any of the tested O_2 concentrations (Figure 1a). Additional studies in BHI showed that again, the Δ*tmpA* mutant grew indistinguishably from WT in all tested O_2 concentrations, whereas the double mutant grew significantly less than its Δ*ssaACB* parent in all tested O_2 concentrations (Figure 1b). BHI contains ~550 nM manganese as compared to ~180 nM measured in rabbit serum (Murgas et al., 2020), which may explain the difference between the mean CFU/ml in each growth medium. These results indicate that TmpA contributes to growth in the Δ*ssaACB* background.

2.3 | Complementation of the Δ*ssaACB* Δ*tmpA* mutant by addition of metals

Although the creation of the Δ*ssaACB* Δ*tmpA* mutant was facilitated by the addition of Mn^{2+} to the media, we wanted to test the effect of addition of Mn^{2+} and other divalent cations on growth of the WT, Δ*ssaACB*, and Δ*ssaACB* Δ*tmpA* strains in serum, used here as a biologically relevant manganese-limited medium. Significant differences in growth of the two mutant strains were observed for every added manganese concentration up to 20 μM (Figure 2). SsaB was also found to transport iron (Crump et al., 2014) and we found that the growth of the Δ*ssaACB* mutant was maximized by the addition of 100 μM Fe^{2+} (Figure 2). Growth of the double mutant was significantly less than the parent in every tested Fe^{2+} concentration. Growth of the two mutant strains was not significantly different in any concentration of added Zn^{2+} (Figure 2), despite the fact that ZIP-family proteins characterized previously primarily transport zinc or iron (Dempski, 2012). These results suggest that TmpA may contribute to both manganese and iron transport in serum.

In another test of complementation with added metals, 24-hr growth of the double mutant on Todd–Hewitt + Yeast Extract (THY) plates required added Mn^{2+} (Figure S1). Neither added Fe^{2+} nor Zn^{2+} had any effect on growth.

2.4 | Complementation of the Δ*ssaACB* Δ*tmpA* mutant with inducible expression of *tmpA*

We next sought to determine whether the phenotype we observed in the Δ*ssaACB* Δ*tmpA* mutant could be complemented. To accomplish this, *tmpA* was placed under the control of a cassette containing the *lacI* gene, the Phyper-spank promoter, and the *lacZo* operator (kindly provided by Dr. David Rudner, Harvard Medical School) at an ectopic chromosomal expression site (Turner et al., 2009) in the double mutant strain. When gene expression was induced by the addition of 1 mM isopropyl-β-D-thiogalactoside (IPTG), the complemented double mutant grew indistinguishably from WT, surpassing the growth of both the Δ*ssaACB* and the Δ*ssaACB* Δ*tmpA* strains (Figure 3). This result indicates that overexpression of *tmpA* leads to an increase in growth compared to WT expression. The addition of 10 μM Mn^{2+} without IPTG to the complemented strain also improved growth to levels that were similar to WT, although significantly lower than the Mn^{2+}-supplemented Δ*ssaACB* mutant. Presumably, this level of complementation is due to leakiness of the

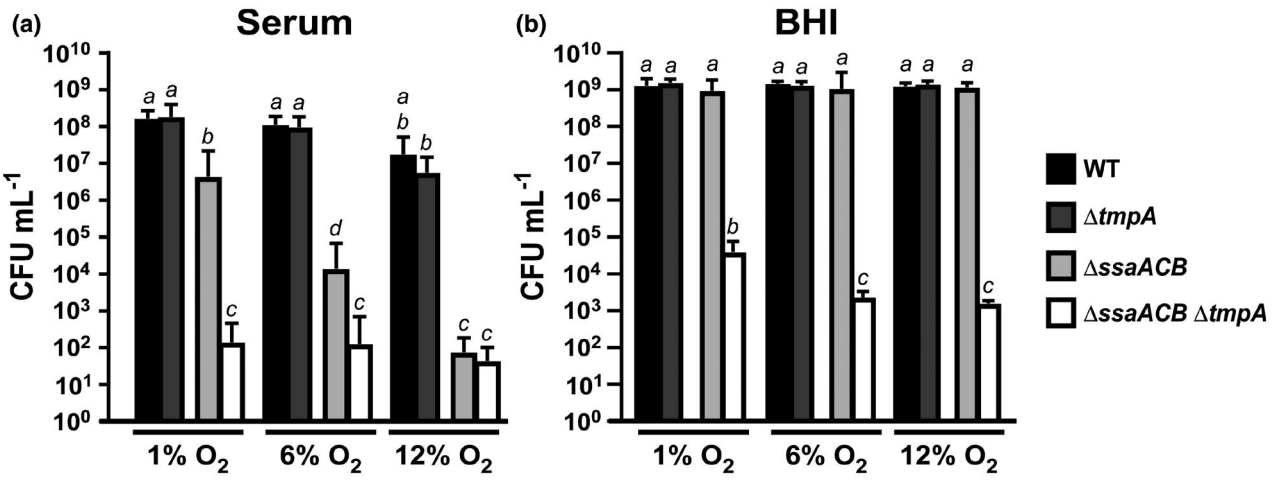

FIGURE 1 Growth of SK36 manganese-transporter mutants in various O_2 concentrations. Cultures were grown in (a) rabbit serum or (b) BHI at the given O_2 concentration for 24 hr. Means and standard deviations of at least three independent experiments are displayed. Significant differences between each Δ*tmpA* mutant and its respective parent strain under the same experimental conditions were determined using one-way ANOVA with a Tukey multiple comparisons post-test. Bars that share a letter in each chart are not significantly different from each other ($p > .05$)

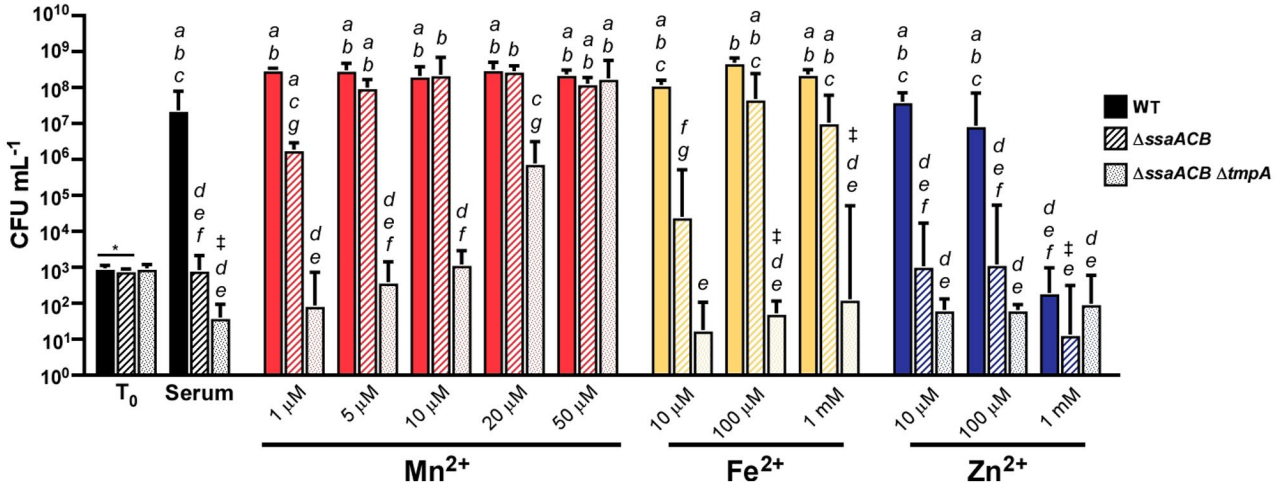

FIGURE 2 Growth of SK36, Δ*ssaACB*, and Δ*ssaACB* Δ*tmpA* mutants in serum with added metals. Cultures were grown in serum at 12% O_2 with added Mn^{2+}, Fe^{2+}, or Zn^{2+} for 24 hr. Means and standard deviations of at least three independent experiments are displayed. Significance was determined by a one-way ANOVA with a Tukey multiple comparisons post-test separately for T_0 and T_{24}. * $p < .05$. Bars that share a letter in each chart are not significantly different from each other ($p > .05$). Bars with ‡ had at least one replicate that fell below the limit of detection

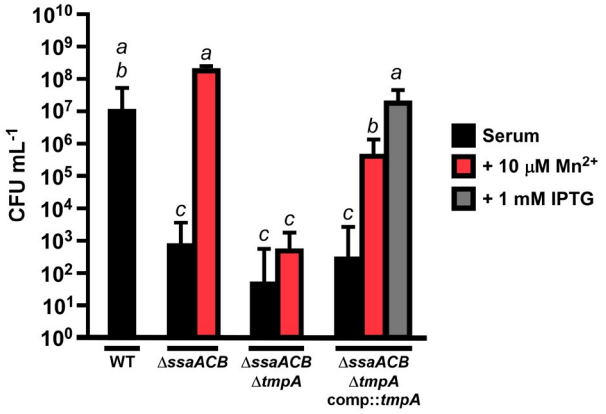

FIGURE 3 Complementation of serum growth of the Δ*ssaACB* Δ*tmpA* mutant. Cultures were grown in serum at 12% O_2 for 24 hr with 10 μM Mn^{2+} or 1 mM IPTG added as shown. Means and standard deviations of at least three independent experiments are displayed. Significance was determined by a one-way ANOVA with a Tukey multiple comparisons post-test. Bars that share a letter in each chart are not significantly different from each other ($p > .05$)

Phyper-spank promoter, leading to considerable expression of *tmpA* even without IPTG present. We have previously observed both high-level expression in the presence of 1 mM IPTG and leaky expression in the absence of IPTG using this same promoter construct located at the same expression site (Rhodes et al., 2014), so neither result is unexpected. These results confirm that the phenotype of the double mutant is due to loss of TmpA rather than any unintended mutation and suggest that even low-level expression of the *tmpA* gene at its native location would be sufficient to augment the growth of the Δ*ssaACB* mutant to the extent indicated in Figure 1. The Δ*ssaACB* mutant was complemented previously (Murgas et al., 2020).

2.5 | Assessment of cellular metal content of Δ*tmpA* mutant strains

We then set out to directly test the effect of *tmpA* deletion on cellular metal concentrations. To assess the metal content of each strain, cells were grown overnight then diluted into aerobic (~21% O_2) BHI with 10 μM of added Mn^{2+}, Fe^{2+}, or Zn^{2+}. The cultures were incubated for several hours, and then cells were collected, washed, digested, and analyzed by inductively coupled plasma optical emission spectroscopy (ICP-OES). There was no significant difference between either Δ*tmpA* mutant and its respective parent strain in plain BHI for any metal tested (Figure 4), including magnesium (Figure S2a). With added Mn^{2+}, the double mutant imported slighty less manganese than the Δ*ssaACB* parent strain (Figure 4b). This trend was not observed for iron or zinc when 10 μM of each respective metal was added (Figure 4d,f). Additionally, there was no difference between each Δ*tmpA* mutant and its parent in magnesium, manganese, iron, or zinc when a different metal was added (Figure S2).

Since the manganese-dependent phenotype of *tmpA* was only observed in the Δ*ssaACB* background, this left the possibility that a zinc-transport phenotype was masked by the presence of high-affinity zinc transporters (AdcCBA and possibly SSA_RS06590 and SSA_RS09740, which encode AdcA homologs). To test this possibility, we first attempted to create a Δ*adcCBA* mutant, deleted for the three adjacent genes encoding the zinc ABC transporter AdcCBA (Dintilhac et al., 1997) but were unsuccessful in obtaining transformants (data not shown). This result indicated that the *adcCBA* operon may be essential for growth. Thus, we decided to generate an Δ*adcC* ATP-binding cassette single gene mutant using the knockout construct from Xu et al. (2011), since in this study, individual mutants of all three components were made successfully, suggesting that deletion of each component separately was tolerated even if deletion

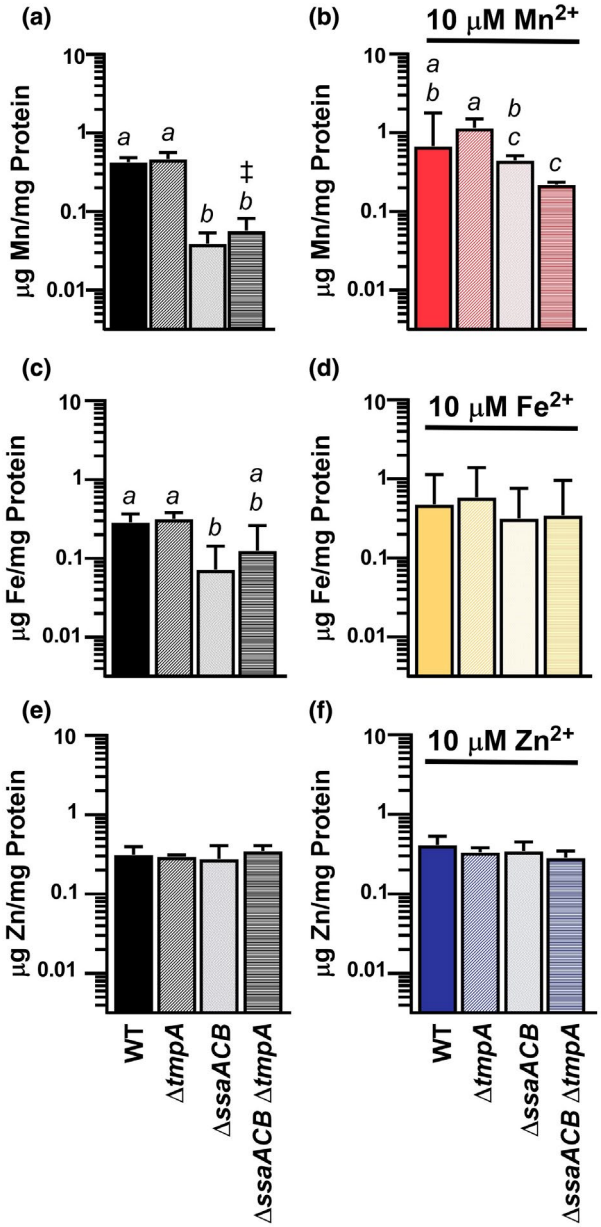

FIGURE 4 Metal content of SK36 manganese-transporter mutants in BHI. Metal content of cells grown in BHI (a,c,e) + 10 μM Mn^{2+} (b), Fe^{2+} (d), or Zn^{2+} (f) in atmospheric O_2 (~21%). Cells were collected at mid-logarithmic phase. Metal concentration was measured by ICP-OES and normalized to protein concentration. Means and standard deviations of at least three independent experiments are displayed. Significance was determined by one-way ANOVA with Bonferonni's multiple comparisons test comparing each mutant and its respective parent in each growth condition. Bars with ‡ indicate that at least one value fell below the lowest standard

of the entire operon was not. Presumably, this is because there is partial redundancy in zinc transport, although we did not investigate this point. As expected, the Δ*adcC* mutant grew normally in BHI (data not shown) and exhibited poor growth in the presence of the metal chelator TPEN when grown in Chelex-treated BHI (cBHI) (Figure S3a). TPEN is often used to reduce available zinc (Ganguly et al., 2021). An Δ*adcC* Δ*tmpA* strain was then created to assess whether TmpA transports zinc in addition to manganese. While both Δ*adcC* strains grew significantly worse than WT, growth of the Δ*adcC* Δ*tmpA* strain was not statistically different from the Δ*adcC* strain in zinc-depleted conditions (Figure S3a). We then evaluated whether there was a difference between the growth of the Δ*adcC* and Δ*adcC* Δ*tmpA* mutants when various concentrations of Zn^{2+} were added to the media and found that there were no significant differences in any added Zn^{2+} concentration (Figure S3b). We then measured the cellular metal content of these mutant strains in cBHI (Figure S3c). There was no significant difference in zinc levels between either Δ*tmpA* mutant and its respective parent, although the slight decrease in the zinc content of the Δ*adcC* Δ*tmpA* strain relative to its parent when 10 μM Zn^{2+} was added suggests that TmpA may make a minor contribution to zinc transport under these conditions.

2.6 | Expression of the *tmpA* gene under various metal and oxygen concentrations

Bacterial metal transporters are often negatively regulated by the metals that they transport, in most cases by binding of the metal to a protein that represses transcription of the transporter gene(s) (Johnston et al., 2006; Kehres & Maguire, 2003). Therefore, as another approach to investigate the metal specificity of TmpA, we investigated the effect of various metals on the regulation of its gene using quantitative reverse transcriptase PCR (qRT-PCR). WT and Δ*ssaACB* cells were grown in BHI and then incubated with 100 μM of either Mn^{2+}, Fe^{2+}, Zn^{2+}, or EDTA (Figure 5a). A BHI-only sample was used as the control for comparison and expression was compared to *tmpA* in BHI alone. Expression of *tmpA* was not significantly affected by the addition of any tested metal nor by the depletion of manganese by EDTA (Figure 5a). The MntR ortholog in *St. sanguinis*, SsaR, has been shown to negatively regulate the expression of *ssaB* in the presence of added manganese (Crump et al., 2014). Thus, the *ssaB* gene and the *aphA-3* (Kan resistance) gene that replaced the *ssaACB* genes in the Δ*ssaACB* mutant were included as positive controls for manganese-dependent regulation and as expected, expression significantly decreased in the presence of added manganese (Figure 5a).

Given that manganese is important in oxidative environments (Waters, 2020), we then assessed whether the expression of *tmpA* was affected by O_2 concentration by measuring transcript levels before and after exposure to oxygen. Expression of *tmpA* did not change significantly from anaerobic to aerobic conditions (Figure 5b). The expression of the positive control *sodA* significantly increased after oxygen exposure, as expected (Crump et al., 2014). Finally, we examined the expression of *ssaB* and *tmpA* in the WT strain under a different set of conditions, including intermediate exposure to oxygen (6% atmosphere) and a longer period of exposure to each metal (~2.5 hr vs. 15 m). Similar to the short-term analysis above, the expression of *tmpA* was unaltered by the addition of excess metals, whereas *ssaB*

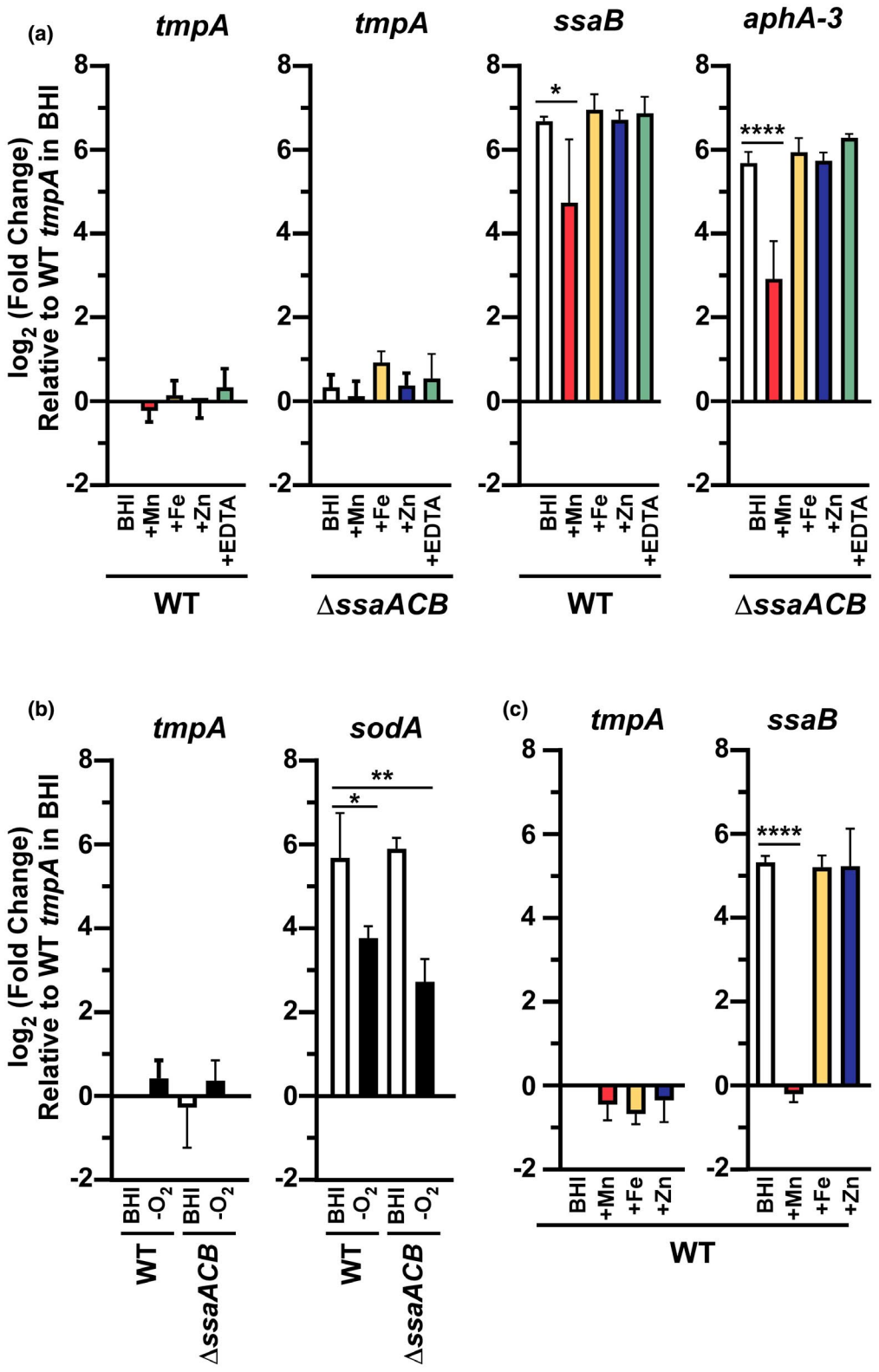

FIGURE 5 Expression of *tmpA* in SK36 WT and Δ*ssaACB* cells when exposed to various metal concentrations and O_2 conditions. Analysis of gene expression by qRT-PCR. Expression of the gene listed above each graph was determined relative to the WT *tmpA* gene in BHI to allow comparison among genes and strains. Means and standard deviations of at least three independent experiments are displayed. Within each group, values were compared by ANOVA followed by Dunnett's multiple comparison test against the BHI control. * $p < .05$; **** $p < .0001$ (a) Effect of 15 m exposure to the metals indicated or EDTA at 100 μM each. (b) Effect of growth in the presence or absence of O_2. (c) Effect of 2.5 hr exposure to the metals indicated at 100 μM

expression was significantly decreased after exposure to excess manganese (Figure 5c). Thus, we have yet to discover a condition that leads to differential expression of *tmpA* and suspect that it may be constitutively expressed. We attempted to assess the production of the TmpA protein in *S. sanguinis* by western blot but were unsuccessful (data not shown). Expression of SsaB in the presence of various divalent cations including those used here was examined by western blot previously with the same result (Crump et al., 2014).

The results shown in Figure 5c indicate that the *ssaB* gene was expressed much more highly than *tmpA* in BHI. This would likely also be true in serum, which is even lower in manganese than BHI (Murgas et al., 2020). This and the results of the complementation experiment (Figure 3) led to the question of whether TmpA's apparent lesser role in manganese transport and serum growth compared to SsaACB is merely a result of its lower level of expression. To test this possibility, we decided to switch the location of each transporter or system so that it would be under the control of the opposite promoter (Figure 6). We began with the Δ*ssaACB* Δ*tmpA* mutant and inserted the *tmpA* gene into the locus where *ssaACB* had been, such that the start of the *tmpA* gene in this strain coincided with the start site of the *ssaA* gene in SK36. This placed the *tmpA* gene under the control of the promoter that is upstream from the *ssaACB* operon (Figure 6a). Likewise, we inserted the *ssaACB* genes into the site where *tmpA* had been. Based on the short distance separating *tmpA* and its upstream neighbors from one another and on the patterns of sequence read mapping to this region in our recent RNA-seq studies (Puccio et al., 2022; Puccio et al., 2020), we believe the *tmpA* promoter lies upstream from SSA_1417 (SSA_RS06950). It is important to note, however, that by placing the *ssaACB* operon in the exact location of *tmpA*, we eliminated the need to identify the native *tmpA* promoter. We first performed qRT-PCR to examine the expression of the *tmpA* and *ssaB* genes in these strains as well as in SK36. As shown in Figure 6b, the *ssaB* gene in the *tmpA* locus was expressed at a level indistinguishable from *tmpA* in the WT strain and vice versa for

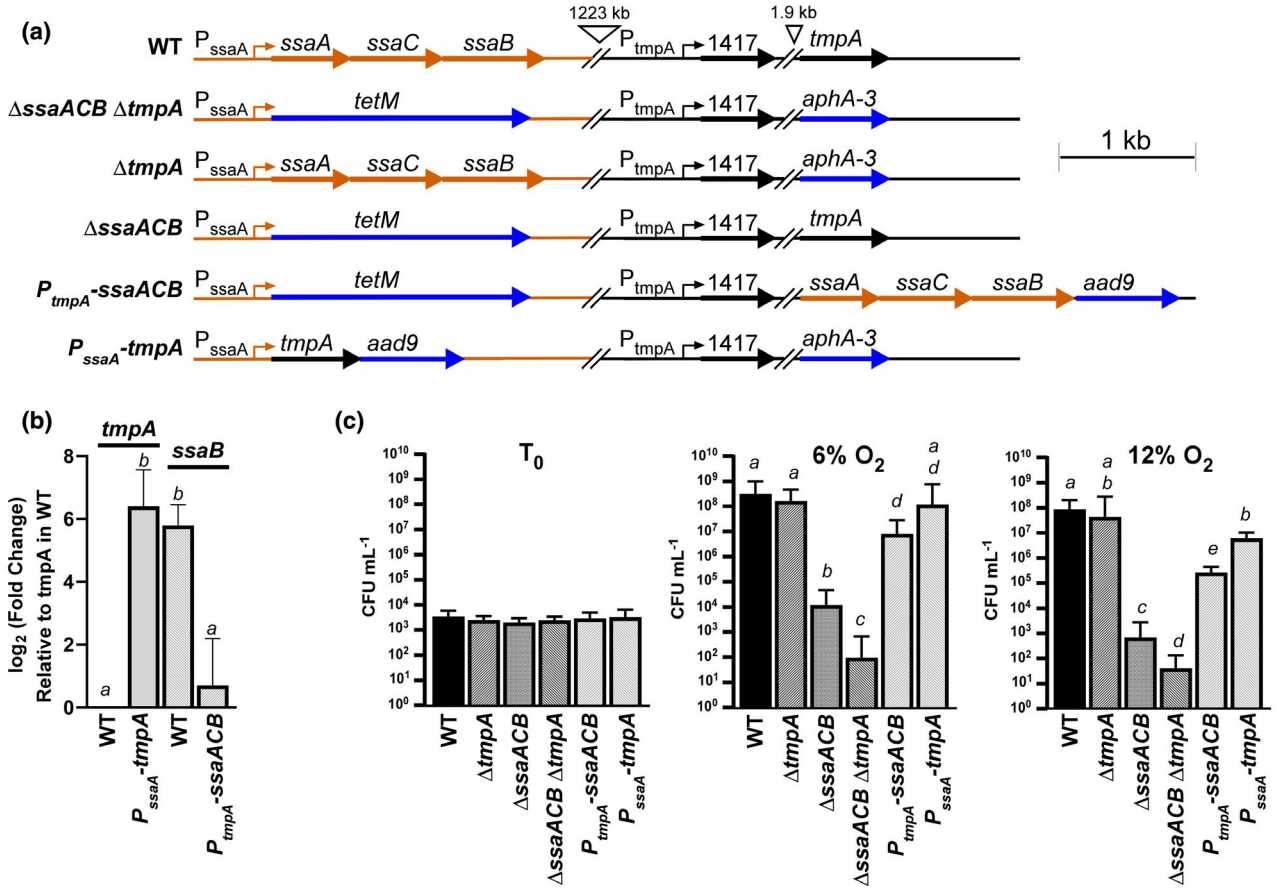

FIGURE 6 Gene expression and growth of strains with promoter-switched manganese-transporter genes. (a) Genetic maps of the six strains employed in this study. Antibiotic resistance markers are indicated in blue; orange and black indicate genes and native flanking regions of the *ssaACB* and *tmpA* gene, respectively. (b) Expression analysis of the *tmpA* and *ssaB* genes in the WT and promoter-switched strains by qRT-PCR. Results are expressed relative to expression of the *tmpA* gene in WT. (c) Growth of the strains depicted in (a) in serum for 0 (T_0) or 24 hr at the oxygen level indicated. In (b) and (c), means and standard deviations obtained from at least three biological replicates are displayed, Significance was determined by one-way ANOVA with a Tukey multiple comparisons test. Bars that share a letter are not significantly different from each other ($p > .05$). P_{tmpA}, the promoter that drives expression of *tmpA* in WT cells, suspected to occur upstream from SSA_1417; P_{ssaA}, the promoter that drives expression of the *ssaACB* operon in WT cells, occurring just upstream from *ssaA*

the *tmpA* gene in the *ssaACB* locus. This confirmed that both genes were being expressed as expected.

We then grew the cells in serum in 6% and 12% oxygen. When each gene was expressed by the other's promoter, the strain with the *tmpA* gene expressed from the *ssaACB* promoter grew to a higher density at 24 hr than the strain in which the *ssaACB* genes were in the *tmpA* locus. This suggests that if the promoters were reversed, TmpA would be the major manganese transporter rather than SsaACB. However, if we compare the strain possessing the *tmpA* gene expressed from the *ssaACB* promoter to the strain possessing the *ssaACB* genes expressed from the *ssaACB* promoter, the SsaACB system supports more growth. The same is true if we compare strains possessing each system expressed from the promoter that normally drives *tmpA* expression. Thus, the lesser contribution of TmpA to manganese transport and serum growth compared to SsaACB is the combined result of lesser activity and lower expression.

2.7 | Contribution of TmpA to virulence in a rabbit model of infective endocarditis

Given the severe reduction in endocarditis virulence of the Δ*ssaB* (Crump et al., 2014) and Δ*ssaACB* (Baker et al., 2019) mutants, we decided to test whether TmpA also contributes to virulence. We employed a rabbit model in which a catheter was inserted through the carotid artery to induce minor aortic valve damage (Turner et al., 2009). Bacterial strains were then introduced into the bloodstream by co-inoculation into a peripheral ear vein. Infected vegetations were recovered the following day from euthanized animals and homogenized. The recovered bacteria were enumerated by dilution plating on selective antibiotics (Turner et al., 2009). Recovery of the Δ*tmpA* mutant was significantly higher than WT and both were recovered in significantly higher numbers than the Δ*ssaACB* strain, which was only detected in vegetations from one of six rabbits (Figure 7a). These results indicate that in a WT background, TmpA is not required for virulence in our model, likely because SsaACB can import sufficient manganese to support growth from the low levels found in blood.

We next wanted to assess the contribution of *tmpA* to virulence in a Δ*ssaACB* background; however, the exceedingly low recovery of the Δ*ssaACB* mutant made it unlikely that a further reduction in virulence would be detectable under these conditions. Therefore, for the next experiment, the WT inoculum level was decreased twofold while the Δ*ssaACB* and Δ*ssaACB* Δ*tmpA* mutant inocula were increased 10-fold, resulting in a 20-fold difference relative to WT. The Δ*ssaACB* strain was recovered from all six rabbits but at a significantly lower level than WT (Figure 7b). The recovery of the Δ*ssaACB* Δ*tmpA* mutant was significantly lower than the Δ*ssaACB* mutant. These results suggest that the loss of TmpA in the Δ*ssaACB* background resulted in a further decrease in virulence, indicating that it may be playing a secondary role in manganese uptake that is only evident when the primary manganese transporter is absent or inactive.

2.8 | Contribution of specific residues of TmpA to its function

To examine the differences between TmpA and other ZIP-family proteins, we aligned the amino acid sequence of TmpA to those of two metal-selective ZIP transporters: ZIPB (zinc) and BmtA (manganese) (Figure S4). We then used Protter (Omasits et al., 2014) to generate a 2D depiction of the protein within a membrane based on the transmembrane domains (TMDs) predicted from the alignment (Figure 8). All ZIP-family proteins characterized thus far have been integral membrane proteins with eight TMDs and are typically predicted to have both C- and N-termini facing extracellularly (Guerinot, 2000). They usually contain two canonical motifs: (a) a variable length $(Hx)_n$ motif in the cytoplasmic loop between TMD III and IV (Eide, 2004) and (b) a conserved HNxPEG motif in TMD IV (Lin et al., 2010). As with BmtA and ZIPB, TmpA has several histidine residues in the variable loop region between TMDs III and IV but only two follow the $(Hx)_n$ pattern. Both protein sequences contain the conserved HNxPEG motif in TMD IV. From the alignment (Figure S4), we found four putative metal-binding residues—E67, N173, E240, and N251—that were different from the confirmed metal-binding residues from the crystal structure of ZIPB (Zhang et al., 2017).

Residue E67 was found near the extracellular side of the protein, while N173 was predicted to be within the central region of the protein (Figure 8) in the "M2" site of the binuclear center (Zhang et al., 2017). Residues E240 and N251 were located in the cytoplasmic loop between TMDs 7 and 8 (Figure 8). Because of the disordered nature of long loops, the main loop between TMDs 3 and 4 was not crystallized; thus, no metal-binding residues were identified in that region of the crystal structure (Zhang et al., 2017). Three of the four residues in TmpA matched those in BmtA (Figure S4). We decided to mutate all four of these residues in TmpA to alanines to determine the contribution of each side chain to the function of the protein (Morrison & Weiss, 2001). We also mutated these four residues to the corresponding residue from ZIPB to determine whether this would affect the function. Since we could not determine a phenotype for the Δ*tmpA* single mutant, we made these site-directed mutants (SDM) in the Δ*ssaACB* background.

We then assessed the growth of these mutants in comparison to WT, the Δ*ssaACB* mutant, and the Δ*ssaACB* Δ*tmpA* mutant in rabbit serum at 6% O_2 (Figure 9a). All E67 and E240 mutants grew similar to the Δ*ssaACB* parent strain, indicating that these residues are not essential for TmpA protein function. N251H also grew indistinguishably from the parent strain but N251A grew significantly worse, which suggests that this residue may be important for transport, but that histidine is also capable of performing the same function. This was not unexpected, as histidine is known to coordinate manganese (Martin & Giedroc, 2016) and the metal-binding residue at position 251 varied between TmpA and BmtA (Figure S4). Both N173 mutants grew poorly, which suggests that this residue is critical for function.

Despite our best efforts, we were unable to detect TmpA by western blot (Puccio, 2020). However, we were able to conclude that tagged protein was still being produced, as strains with the

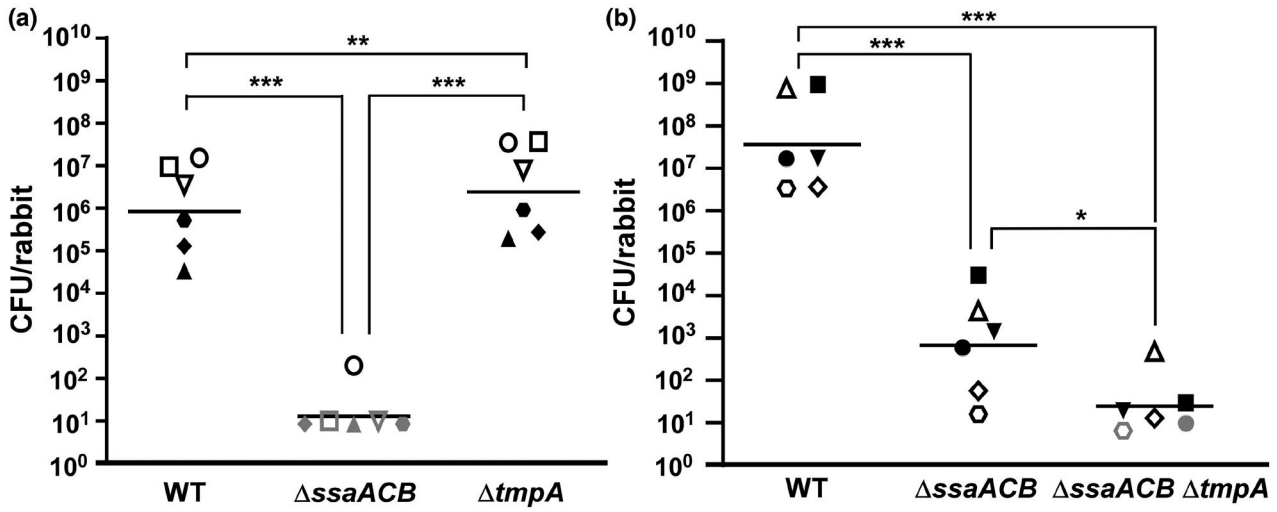

FIGURE 7 Virulence of SK36 manganese-transporter mutants in a rabbit model of IE. Rabbits were co-inoculated with the marked WT strain, the Δ*ssaACB* mutant, and either (a) the Δ*tmpA* or (b) the Δ*ssaACB* Δ*tmpA* mutant strain. In (a), the inoculum sizes for the three strains were approximately equal and normalized to inocula for each experiment. In (b), the inoculum for WT was 20 times lower than the inoculum of each Δ*ssaACB* mutant, thus final recovery was multiplied by 20 to normalize to the inocula of the other two strains. Within each panel, like symbols indicate bacteria of each strain recovered from the same animal ($n = 6$ over two independent experiments). Females are represented by open symbols and males are represented by closed symbols. Gray symbols indicate recovery was below the limit of detection. Horizontal lines indicate geometric means. $^{*}p \leq .05$, $^{**}p \leq .01$, $^{***}p \leq .001$ indicate significant differences using repeated-measures ANOVA with a Tukey multiple comparisons test

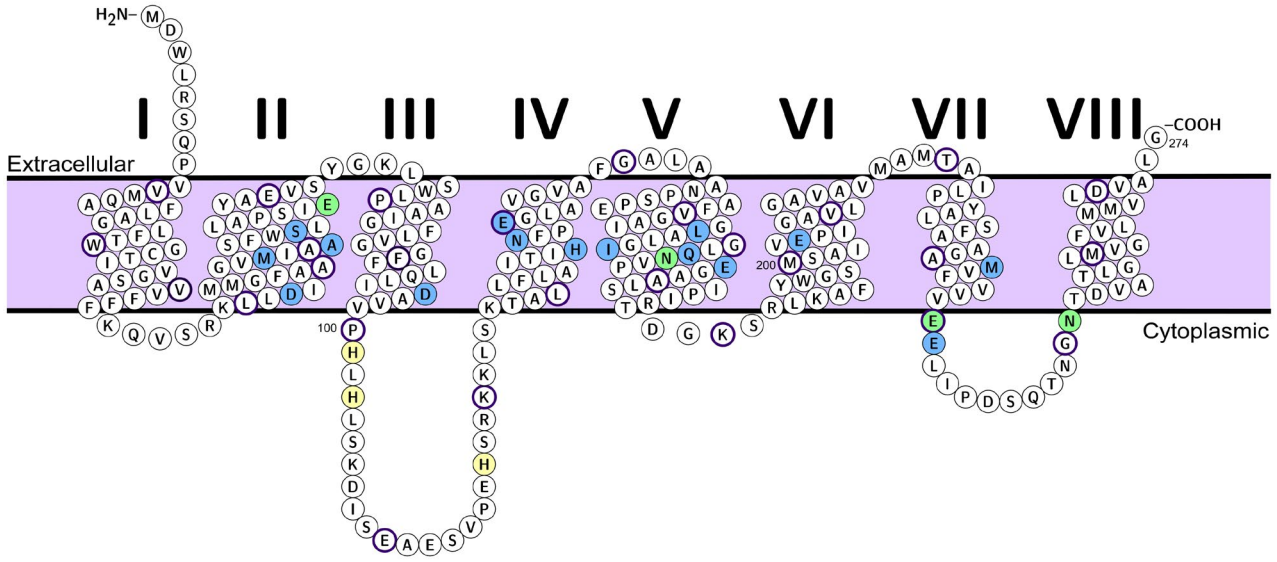

FIGURE 8 Depiction of predicted TmpA tertiary structure within a membrane. TmpA amino acid sequence depicted in a cell membrane using Protter (Omasits et al., 2014). TMDs of TmpA were predicted based on alignment to the crystal structure of ZIPB (Figure S4). Every 10th residue is circled in dark purple. Amino acids in blue and green are conserved putative metal-binding residues based on the crystal structure of ZIPB bound to zinc (Zhang et al., 2017). The four green residues are metal-binding residues that are not conserved between ZIPB and TmpA. Yellow residues in loop 3 are histidines thought to contribute to metal transport (Zhang et al., 2019) but have not been confirmed by the crystal structure

Strep-Tag® II tag fused to TmpA at two different sites grew similar to the parent strain when 5 μM Mn^{2+} was added (Figure S5). The clear exception was the N-terminally tagged version, which suggests that the N-terminus may be important either for function or for localization to the membrane. Additionally, we attempted to overexpress the TmpA protein in *Ec. coli* strains optimized for heterologous membrane protein expression. While we were able to confirm the presence of recombinant TmpA by western blot (Puccio, 2020), we were unsuccessful in obtaining sufficient protein quantities to perform cell-free transport assays in liposomes,

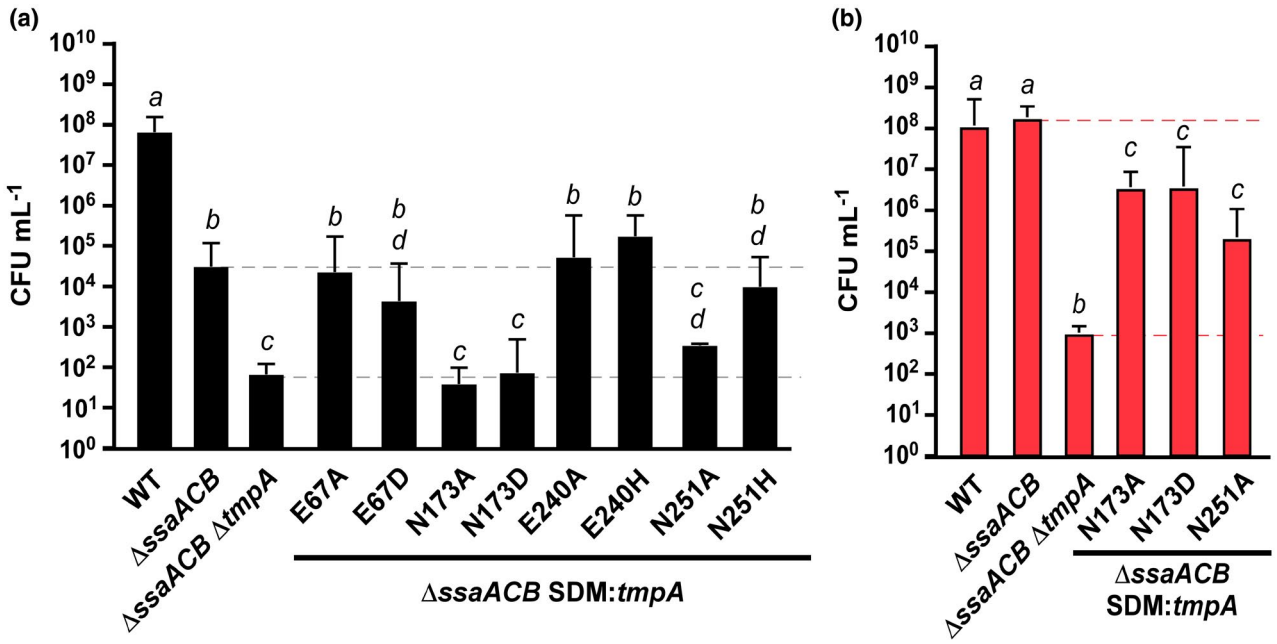

FIGURE 9 Growth of Δ*ssaACB* SDM:*tmpA* mutants. (a) Growth of single amino acid (site-directed mutagenesis; SDM) mutant versions of TmpA in the Δ*ssaACB* background was assessed in serum at 6% O_2. (b) Mutants deficient in growth as compared to the Δ*ssaACB* parent at 6% O_2 in (a) were evaluated for growth under the same conditions + 5 μM Mn^{2+}. Means and standard deviations of at least three independent experiments are shown. Significance was determined by one-way ANOVA with a Tukey multiple comparisons test. Bars that share a letter are not significantly different from each other ($p > .05$). Horizontal lines are for reference to parent strain growth

which would have been ideal for measuring the contribution of each residue to metal transport.

We thus considered two extreme explanations for the failure of the N173A, N173D, and N251A mutants to display growth that was significantly better than the Δ*ssaACB* Δ*tmpA* mutant in Figure 9a: (a) the N173 and N251 mutations interfered with the secretion, localization, or stability of TmpA; or (b) the SDM were normal with regard to these properties, and their lack of detectable activity was due to the importance of these residues for manganese transport. To distinguish between these two possibilities, the three mutants that grew poorly in serum in 6% O_2 were assessed for growth after the addition of 5 μM Mn^{2+} (Figure 9b). When Mn^{2+} was added, the Δ*ssaACB* parent grew to WT-like levels, whereas the Δ*ssaACB* Δ*tmpA* mutant's growth was still significantly lower than WT. Each of the mutants grew to a level that was lower than the Δ*ssaACB* parent but higher than the Δ*ssaACB* Δ*tmpA* mutant. The results for all three SDM are in agreement with the second model, in which the lack of activity in unamended serum is due to reduced metal transport rather than loss of the protein.

2.9 | Model of TmpA based on the ZIPB crystal structure

To determine whether the two N173 mutations would be expected to severely affect metal transport function, we modeled TmpA using the crystal structure of ZIPB as a template (Figure S6a). The full-length proteins share 40% identity, while the crystal structure of ZIPB (PBD: 5TSA) shares 34% identity with TmpA due to lack of structural data for several loops. Additionally, TMD III in TmpA was shorter than that of ZIPB, and thus was depicted missing one of the helical loops in the model (Figure S6a). The reason for this short TMD is unclear, as the length of all other TMDs appear to match well.

We then modeled the N173D mutation in TmpA (Figure S6b). The other residues that constitute the putative M2 binding site moved to accommodate the negative charge of the aspartic acid, which resulted in a change in the size and shape of the M2 site. The change in shape and size is, of course, speculative, as proteins in vivo are flexible and may be able to accommodate changes such as these. Nevertheless, the predicted structural changes, in conjunction with the obvious change in charge, could well explain the severity of this mutation's effect on metal transport and growth observed in Figure 9.

The position of the proteins within the cellular membrane was then predicted using Orientation of Proteins in Membranes (https://opm.phar.umich.edu/). As described in Zhang et al. (2017), the protein has been crystallized with a tilt (Figure S7a). The model of TmpA fits well in the predicted membrane with this tilt (Figure S7b).

2.10 | Sequencing of the SK36 Δ*ssaACB* Δ*tmpA* double mutant

After completing most of the experiments in this manuscript, we sequenced the whole genomes of the Δ*ssaACB* mutant (JFP173) and the Δ*ssaACB* Δ*tmpA* mutant (JFP227). Unfortunately, we discovered

the presence of a nonsense mutation in SSA_1414 (W139*) in JFP227. SSA_1414 is annotated as MutT, an 8-oxo-dGTP diphosphatase. We confirmed this mutation by Sanger sequencing and found that it was unique to this strain, as it was not present in the Δ*tmpA* single mutant (JFP226), which was made with the same PCR product as JFP227. We recreated markerless versions of this mutation in the WT and Δ*ssaACB* backgrounds and found no significant differences in serum growth for either version (Figure S8). We next generated a clean Δ*ssaACB* Δ*tmpA* strain and confirmed by Sanger sequencing that the SSA_1414 gene was intact. We compared the growth of this new mutant (JFP377) to that of JFP227 (Figure S9a–c) under various conditions. There was no significant difference in growth between these strains. We then measured the metal content of cells grown in BHI with 10 μM Mn^{2+} using ICP-OES and observed no significant difference in any metal examined (Figure S9d).

2.11 | Evaluation of serum growth of manganese-transporter mutants in additional *St. sanguinis* strains

Given the considerable genotypic and phenotypic heterogeneity that we previously observed between different strains of *St. sanguinis* (Baker et al., 2019), we wanted to determine whether our findings concerning manganese transport in SK36 would apply to other strains as well. We, therefore, examined the manganese transporters in four additional *St. sanguinis* strains: SK49, SK408, SK678, and VMC66. Like SK36, SK49 is an oral isolate. By ICP-OES, we found previously that it accumulated less manganese when cultured in BHI than 14 of the 17 strains examined (Baker et al., 2019). VMC66 (Kitten et al., 2012), SK408, and SK678 were all isolated from the blood of endocarditis patients and ranked first, second, and third, respectively, in manganese levels in the same assay (Baker et al., 2019).

Manganese transporter mutants—Δ*ssaACB*, Δ*tmpA*, and Δ*ssaACB* Δ*tmpA*—were generated for each strain. These mutants and their parent strains were then assessed for serum growth at 6% O_2 (Figure 10). As with SK36 (Figure 1a), all Δ*tmpA* mutant strains were indistinguishable from WT and all Δ*ssaACB* strains were deficient for growth. Interestingly, the Δ*ssaACB* Δ*tmpA* mutants of SK678 and VMC66 grew similar to their respective Δ*ssaACB* parent strains, whereas the SK49 and SK408 versions grew to significantly lower densities than their parent strains. However, it is apparent that in SK678 and VMC66, the *ssaACB* deletion produced a greater defect on growth than in the other backgrounds (Figure 10c,d).

To determine if the poor growth of the Δ*ssaACB* parents prevented us from detecting an additional effect of *tmpA* deletion, growth of SK678, VMC66, and their derivatives was assessed in 1% O_2 (Figure S10). Under these conditions, we observed a significant difference between each Δ*ssaACB* Δ*tmpA* mutant and its Δ*ssaACB* parent. In summary, the mutant phenotypes observed in the SK36 background were similar to those of mutants in other strains of *St. sanguinis*.

2.12 | Relative contribution of TmpA and MntH to growth and virulence of *St. sanguinis* VMC66

Of interest to this study, at least eight *St. sanguinis* strains with genome sequences available in GenBank encode gene orthologous to the NRAMP protein MntH found in *St. mutans* (Kajfasz et al., 2020) and other gram-positive bacteria (Kehl-Fie et al., 2013). NRAMP proteins are known to import manganese (Bozzi et al., 2016; Ehrnstorfer et al., 2014) and contribute to endocarditis virulence in *Enterococcus faecalis* (Colomer-Winter et al., 2018). It was unexpected then that the VMC66 Δ*ssaACB* mutant performed so poorly in the 6% O_2 serum growth study given that VMC66 encodes two secondary Mn transporters (Figure 10d). To determine whether these NRAMP proteins may contribute to manganese uptake and endocarditis virulence in *St. sanguinis*, knockout mutants were generated in the VMC66 WT and Δ*ssaACB* strains, and serum growth was assessed. At 6% O_2, the Δ*mntH* strain grew to a significantly lower level than

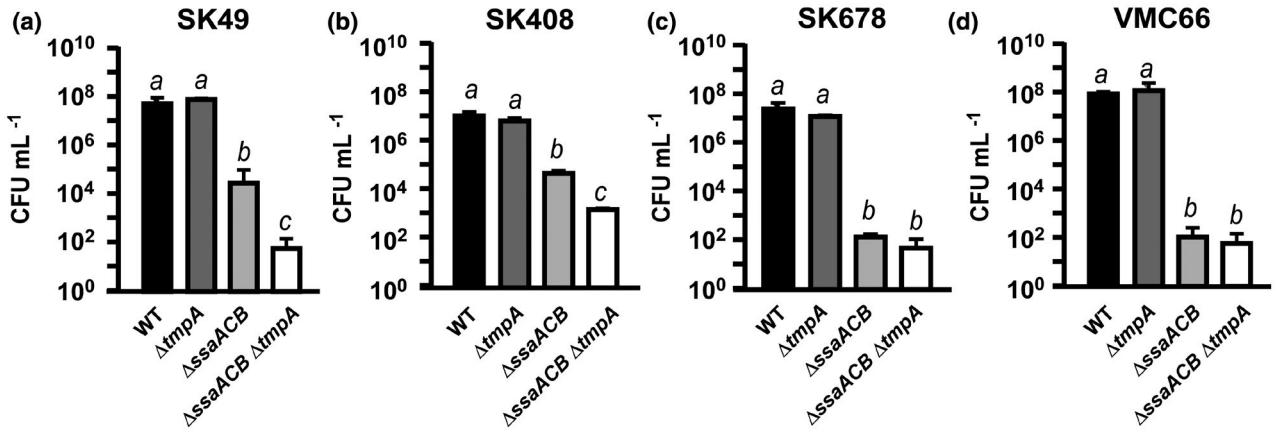

FIGURE 10 Growth of manganese-transporter mutants of other *Streptococcus sanguinis* strains. Growth of each strain and its respective mutants in serum at 6% O_2 was assessed by plating on BHI agar at 24 hr. Means and standard deviations of at least three independent experiments are displayed. Significance was assessed by one-way ANOVA with a Tukey multiple comparisons test. Bars that share a letter within a chart are not significantly different from each other ($p > .05$)

the WT parent but higher than the Δ*ssaACB* mutant (Figure 11a). Both double mutant strains grew similar to their Δ*ssaACB* parent (Figure 11a).

These results indicate that MntH can contribute to growth even in cells possessing the other two transporters, but its contribution is much less than that of SsaACB. As seen in Figure 10, the drastic growth reduction in the Δ*ssaACB* mutant masked the contribution of TmpA in this background at 6% O_2 and this could have been true in this experiment for MntH as well. Thus, we decided to assess growth at 1% O_2 (Figure 11b). When we lowered the oxygen concentration, we once again observed that the Δ*ssaACB* Δ*tmpA* mutant of VMC66 grew significantly worse than the Δ*ssaACB* parent. Both Δ*mntH* and Δ*ssaACB* Δ*mntH* grew to slightly but not significantly lesser densities than their respective parent strains.

We then assessed the relative contribution of each secondary transporter to manganese import by measuring cellular metal content by ICP-OES (Figure 11c). We found that there were no significant differences between the manganese content of either Δ*tmpA* mutant and its respective parent strain under either condition (Figure 11c,d). The same was true of other tested metals: iron, zinc, and magnesium (Figure S11). However, manganese levels in the Δ*ssaACB* Δ*mntH* mutant were significantly lower than in the Δ*ssaACB* parent, suggesting that MntH contributes more to manganese transport in this background (Figure 11c).

To determine the relative contribution of each manganese transporter to VMC66 virulence, WT, Δ*tmpA*, Δ*ssaACB*, *and* Δ*mntH* strains were tested in our rabbit model of IE (Figure 12a). To selectively plate the WT, we utilized a VMC66 Spc^R WT strain generated previously (Baker et al., 2019). The Δ*mntH* mutant was recovered at similar levels to this marked WT strain. The only strain to be recovered at significantly lower levels than WT was the Δ*ssaACB* strain, highlighting its importance as the primary manganese transporter in multiple *St. sanguinis* strains.

To test the relative contribution of each secondary transporter to virulence, the double mutants were also tested in our IE rabbit model (Figure 12b). To ensure sufficient recovery of the Δ*ssaACB* mutants, we once again increased the inoculum size of each of these mutants and decreased the inoculum size of WT so that the WT inoculum was twenty times less than that of the three mutants. We were able to recover colonies of every strain from each rabbit and we saw a significant difference between the WT and both double mutant strains. However, the difference between WT and the Δ*ssaACB* mutant fell short of significance (p-value = .0589). We observed a significant difference between the Δ*ssaACB* Δ*tmpA* mutant and its parent but neither was significantly different from the Δ*ssaACB* Δ*mntH* mutant. This suggests that TmpA may contribute to virulence, even when MntH is present.

Given the results shown in Figures 11 and 12, it appears that TmpA and MntH each contributed to manganese transport, serum growth, and/or endocarditis virulence in the VMC66 background, with the magnitude of the contribution differing depending on the assay. We, therefore, decided to create a triple mutant lacking all three transporters and examine it in a serum growth study. As can be seen in Figure 13, the triple mutant's growth was not statistically different from that of the Δ*ssaACB* Δ*mntH* double mutant in 12% O_2, whether growth was in unamended serum or serum to which 1 or 50 μM Mn^{2+} had been added. As will be discussed below, this strain possessed a growth defect that was not discernible in this assay; nevertheless, it is clear that even when every known manganese transporter has been deleted from this strain (Figure 13) or SK36 (Figures 2 and 4), there is likely at least one additional unknown manganese transporter in each strain. Identification of the transporter(s) will await future studies.

2.13 | Phylogenetic analysis of TmpA homologs

We next wanted to assess the phylogenetic distribution of the TmpA open reading frame (ORF) in streptococci, beginning with *St. sanguinis*. By BLASTP or TBLASTN analysis (Altschul et al., 1990), all *St. sanguinis* strains with complete genomes contained a clearly identifiable *tmpA* allele. Interestingly, however, in a minority of cases, it was a pseudogene due to the presence of a single, internal, in-frame stop codon. A TmpA homolog was present in many other streptococcal species for which at least one complete genome sequence was present. Exceptions included *Streptococcus pneumoniae*, *Streptococcus mitis*, *Streptococcus oralis*, *Streptococcus pyogenes*, and *Streptococcus vestibularis*, all of which appear to lack a TmpA homolog or contain only partial sequences. Additionally, a phylogenetic analysis showed that previously characterized ZIP proteins from other genera of bacteria, such as BmtA and ZIPB, were more closely related to the main group of streptococcal ZIP proteins than were the homologs from *St. mutans* and *Streptococcus ratti* (Figure S12a). The TmpA homolog of *Streptococcus sobrinus*, a member of the "Mutans" group of streptococci (Nobbs et al., 2009), also clustered with the main group of streptococcal proteins rather than with those from *St. mutans* and *St. ratti*. ZupT proteins from *Ec. coli* and *C. difficile* were more similar to the *St. mutans* protein than to TmpA from *St. sanguinis*. Furthermore, we included the human ZIP-family proteins hZIP11 and hZIP8 for use as outgroups. We found that hZIP11 was more closely related to most of the bacterial ZIP-family proteins than were those of *St. mutans* and *St. ratti*, whereas the hZIP8 protein functioned as a true outgroup. These results, along with the observation that our ZIP protein phylogenetic tree looks very different from a 16S rRNA-based tree (Nobbs et al., 2009), indicate that genes encoding ZIP-family proteins were likely incorporated into the genome of each species or various progenitors at different times, which has been observed previously in streptococci, as opposed to being derived from a common ancestor (Richards et al., 2014). The GC content of the *St. sanguinis* genome is 43.40% (Xu et al., 2007) whereas *tmpA* is 50.42%, indicating that it could have been acquired by horizontal gene transfer (Ravenhall et al., 2015).

As a comparison, we evaluated the phylogeny of SsaB orthologs in streptococci (Figure S12b). Most species contained orthologs of SsaB, including those that were lacking a ZIP-family protein, such as *St. mitis*, *St. oralis*, *St. pyogenes*, and *St. vestibularis*. Interestingly,

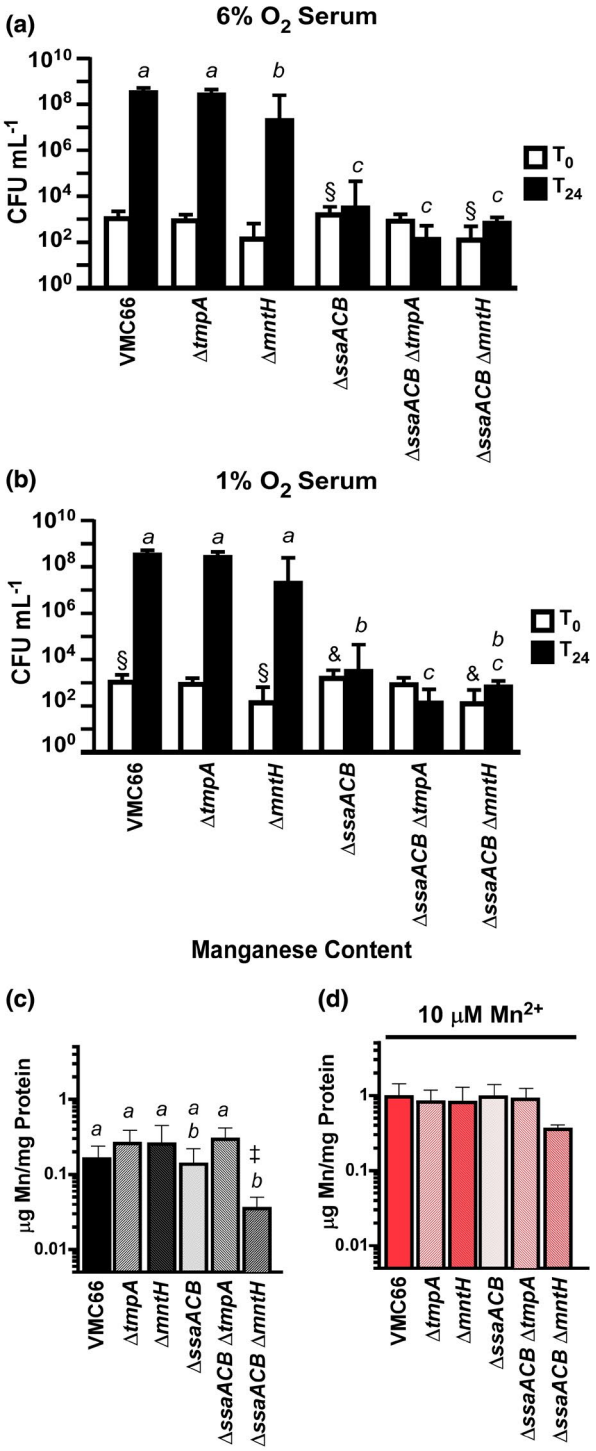

FIGURE 11 Growth and manganese content of VMC66 manganese-transporter mutants. Growth of VMC66 and its respective manganese-transporter mutants in serum at (a) 6% O_2 and (b) 1% O_2 was assessed by plating on BHI agar after 24 hr. Means and standard deviations of at least three independent experiments are displayed. Significance was assessed by one-way ANOVA with a Tukey multiple comparisons test for T_0 and T_{24} separately. T_{24} bars that share a letter within a chart are not significantly different from each other ($p > .05$). T_0 bars with § or & are significantly different from each other ($p \leq .05$). (c) Manganese content of each strain in BHI ± 10 μM Mn^{2+} was measured by ICP-OES and normalized to protein concentration. Means and standard deviations of at least three independent experiments are displayed. Significance was determined by one-way ANOVA with Tukey multiple comparisons post-test. Bars that share a letter within a chart are not significantly different from each other ($p > .05$). The ‡ indicates that at least one replicate was below the lowest standard

Streptococcus suis and *St. ratti* lack an SsaB ortholog. *St. mutans* again groups separately from the rest of the streptococci (100% of 500 replicate trees inferred by bootstrap analysis), including another "Mutans" group *Streptococcus*, *St. downei*, but the *St. mutans* ortholog (SloC) clusters more closely with the other streptococcal proteins than do representatives from more distantly related species. We then looked closer at the *St. mutans* ZIP protein, $ZupT_{Sm}$. When we performed a BLASTP search with $ZupT_{Sm}$ as the query, most of the hits were either other Firmicutes or streptococcal species that are closely related to *St. mutans* (Figure S13). A similar search performed with TmpA identified γ-proteobacteria and firmicutes of different genera from those identified in the $ZupT_{Sm}$ search. These analyses further support the independent incorporation of TmpA/ZupT orthologs in *St. mutans* and the other streptococci at different times and likely from different sources.

3 | DISCUSSION

With this study, it has now been confirmed that at least two different bacterial species, *St. sanguinis* and *B. burgdorferi*, utilize a ZIP-family protein for manganese uptake. This firmly establishes the ZIP family as an additional bacterial manganese importer family. Additionally, we confirm that an NRAMP-family protein, MntH, contributes to manganese uptake in at least one *St. sanguinis* strain in which it is naturally encoded. These findings confirm the existence of secondary manganese transporters in *St. sanguinis*. Despite the fact that there was an unintended mutation in the Δ*ssaACB* Δ*tmpA* mutant in a nearby gene, SSA_1414, we were able to demonstrate that a clean mutant shares the same phenotype (Figure S9) and that the Δ*ssaACB* Δ*tmpA* mutant could be complemented by the expression of the *tmpA* gene at a different chromosomal site (Figure 3).

We showed that the Δ*ssaACB* mutant accumulates less iron and manganese, in agreement with our previous results (Crump et al., 2014; Murgas et al., 2020). The findings that low levels of manganese restore serum growth to the Δ*ssaACB* mutant, that higher manganese levels are required for restoration of growth to the Δ*ssaACB* Δ*tmpA* mutant, and that less cellular manganese is detected in the Δ*ssaACB* Δ*tmpA* mutant compared to its Δ*ssaACB* parent are all consistent with the conclusion that TmpA transports manganese and that this activity is important in the background of an Δ*ssaACB* mutant. The finding that supplemental iron restores serum growth to the Δ*ssaACB* mutant has not been reported previously, although in our earlier paper we did not attempt complementation with more than 10 μM supplemental iron, and we reported that it did not reproducibly restore growth (Crump et al., 2014), which is not

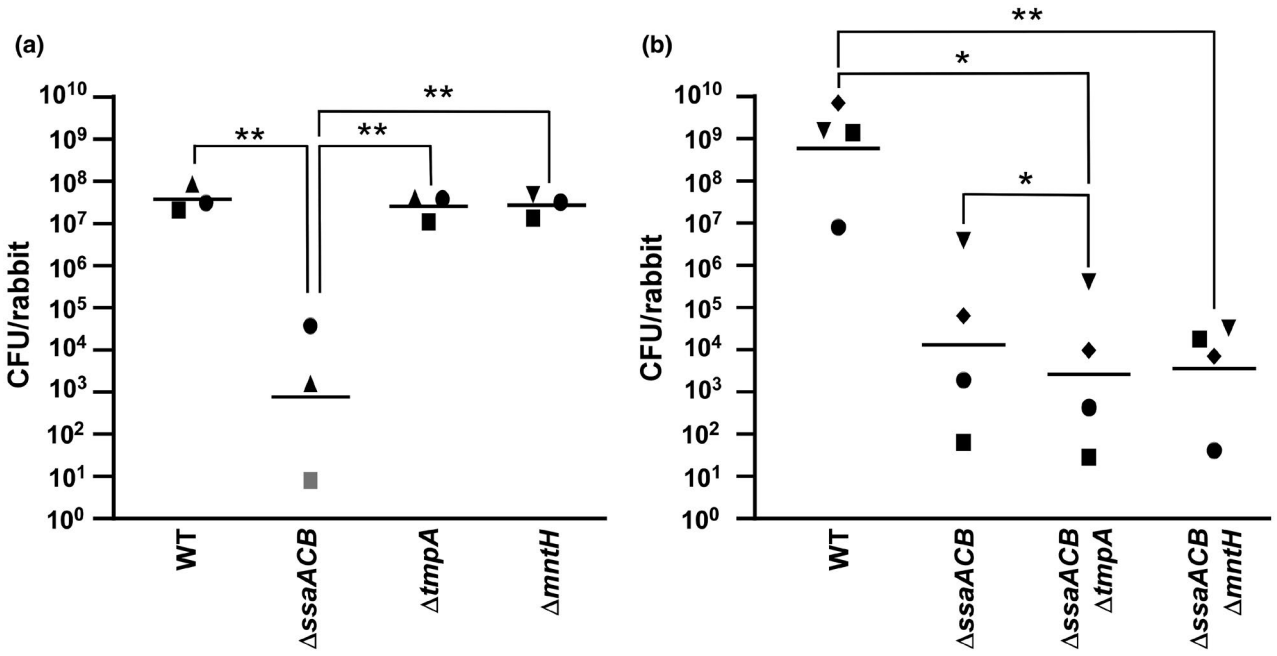

FIGURE 12 Virulence of VMC66 manganese-transporter mutants in a rabbit model of IE. Rabbits were co-inoculated with the marked WT strain, the Δ*ssaACB* mutant strain, and either (a) the Δ*tmpA* and Δ*mntH* single mutant strains or (b) the Δ*ssaACB* double mutant strains. In (a), the inoculum sizes for the three strains were approximately equal and normalized to inocula for each experiment. In (b), the inoculum for WT was 20 times lower than the inoculum of each Δ*ssaACB* mutant, thus final recovery was multiplied by 20 to normalize to the inocula of the other two strains. Within each panel, symbols of the same shape indicate bacteria of each strain recovered from the same animal, where (a) $n = 3$ and (b) $n = 4$. All rabbits were male. Gray symbols indicate recovery was below the limit of detection. Geometric means are indicated by horizontal lines. $^{*}p \leq .05$, $^{**}p \leq .01$ indicate significantly different from other strains using repeated-measures ANOVA with a Tukey multiple comparisons test

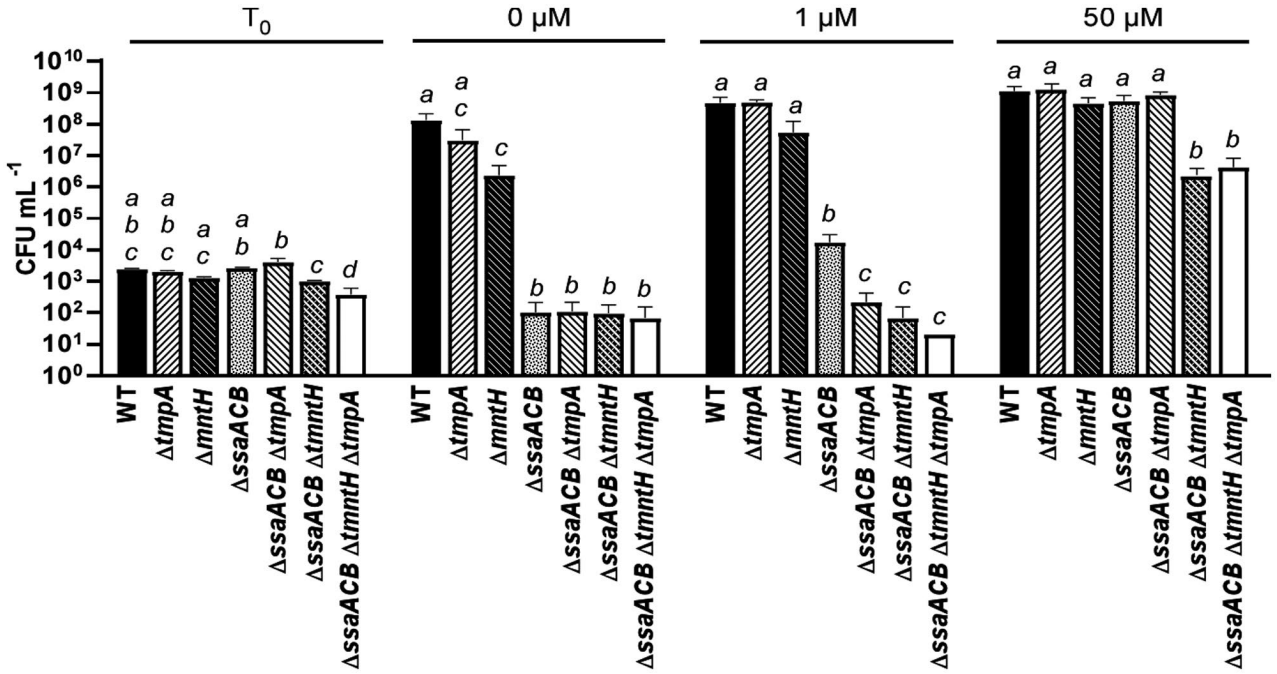

FIGURE 13 Serum growth of VMC66, single, double, and triple mutant strains. The strains indicated were grown in an atmosphere of 12% O_2 for 0 (T_0) or 24 hr in pooled rabbit serum containing 0, 1, or 50 μM added Mn^{2+} as indicated. Means and standard deviations of at least three independent experiments are displayed. Significance was assessed separately for each time or condition by one-way ANOVA with a Tukey multiple comparisons test. Bars that share a letter within a chart are not significantly different from each other ($p > .05$)

inconsistent with our findings from this study. It thus appears that supplemental iron is capable of restoring serum growth, although the levels required are perhaps ~20-fold greater than required for manganese. We presume that mononuclear iron is substituting for manganese as a cofactor in enzymes that can use either metal (Anjem & Imlay, 2012).

The effects of the Δ*tmpA* mutation in relation to iron are less easily understood than the effects on manganese. We found that, as with manganese, the deletion of *tmpA* from the Δ*ssaACB* mutant resulted in iron being less effective at restoring serum growth; indeed, while ~20-fold more manganese was required to restore growth to the double mutant relative to its parent, no amount of added iron (up to 1 mM) was sufficient to restore growth. This result could suggest that TmpA is a secondary transporter of iron as well as manganese and that unlike manganese, which we presume is transported into the double mutant by one or more tertiary transporters, there is no tertiary transporter for iron under these conditions. Yet, unlike with manganese, the Δ*ssaACB* Δ*tmpA* double mutant and its Δ*ssaACB* parent were indistinguishable with regard to iron uptake in the presence or absence of supplemental iron (Figure 4), which is inconsistent with TmpA-mediated iron transport under these conditions.

We suggest that these seemingly inconsistent findings can be explained by hypothesizing that there are certain core functions that require manganese, and no amount of iron can restore growth if manganese levels are insufficient to meet these needs. Therefore, the failure of iron to complement the double mutant is due to the loss of TmpA-mediated manganese transport rather than TmpA-mediated iron transport. If we presume that increased levels of manganese are needed for the core functions as levels of oxygen and, therefore, oxygen-dependent reactive oxygen species such as superoxide and hydrogen peroxide increase (Anjem & Imlay, 2012), this would also be consistent with the data in Figure 1 showing that as oxygen levels decrease, the Δ*ssaACB* mutant is capable of ever more growth in serum. It should also be noted that particularly in blood, if not also in the oral cavity, free iron is present in vanishingly low levels (Diaz-Ochoa et al., 2014); thus, the significance of iron transport by the SsaACB transporter is not clear.

Despite the fact that most ZIP-family proteins transport zinc, there were no significant differences between any Δ*tmpA* mutant and its respective parent in either zinc levels or zinc-deficient growth. Any difference in zinc levels between the Δ*adcC* and Δ*adcC* Δ*tmpA* mutants with 10 μM added Zn^{2+} was insignificant and given that this concentration is likely biologically unattainable, the combined data suggest that zinc transport, if any, is minimal. We recognize, however, that transport of other metals including zinc and iron by TmpA may occur under conditions we have not tested. Moreover, in vitro studies with liposomes or similar approaches would be required to completely rule out the possibility of zinc or iron transport by TmpA.

We have been unable to find a differential phenotype for the Δ*tmpA* single mutant as compared to WT, with the exception of a slight increase in endocarditis virulence (Figure 7a). In our accompanying manuscript (Puccio et al., 2022), we tested its growth in low-pH BHI and saw no significant differences. We also assessed the growth in a biofilm assay in competition with *St. mutans* and observed no difference (data not shown). These results, along with those described in this study, strongly suggest that TmpA function is secondary to SsaACB.

The reason that most organisms encode multiple transporters for each metal is still contested, although it highlights the importance of these transition metals. The presence of multiple transporters with varying affinity could be due to the transport systems functioning optimally under different environmental conditions or it could protect from the loss of function of one of the transporters (Dempski, 2012; Eide, 2012; Raimunda et al., 2011). For example, excess zinc was found to inhibit the manganese transport function of the SsaB ortholog in *St. pneumoniae*, PsaA (Counago et al., 2014). If this is also true for SsaB, TmpA's function could become essential under the same condition. In our accompanying manuscript (Puccio et al., 2022), we found that loss of Δ*ssaACB* was detrimental to growth in low-pH media, which we hypothesize is due to acid sensitivity of TmpA. In VMC66, lack of Δ*ssaACB* had no effect in the same conditions, likely because MntH is still functional at the pH tested. Further studies will be required to confirm the identity and selectivity of other metal transporters in *St. sanguinis*.

In VMC66, the only single manganese transport system mutant that showed significantly decreased virulence was the Δ*ssaACB* mutant (Figure 12a). The Δ*ssaACB* Δ*tmpA* mutant was recovered at significantly lower levels than the Δ*ssaACB* mutant whereas the Δ*ssaACB* Δ*mntH* mutant was not. However, when the two double mutants were compared to each other, they were not significantly different (Figure 12b). Thus, we cannot confidently conclude that the Δ*tmpA* mutation had a greater effect on the virulence of the Δ*ssaACB* mutant than the Δ*mntH* mutation did. Nevertheless, the contribution of these manganese transport systems should be further evaluated in relation to other bacterial species that cause IE as well as other infectious diseases. For instance, a related IE pathogen, *En. faecalis*, encodes a SsaACB ortholog as well as two MntH proteins that have functional redundancy but play different roles in disease (Colomer-Winter et al., 2018). These studies suggest that selective pressure has retained functionally redundant transport systems to improve survival in diverse environments.

Expression of *tmpA* was not significantly affected by the addition of metals or by depletion with EDTA, whereas expression of *ssaB* decreased after exposure to manganese at both 15 min and 2.5 hr. Nor was expression affected by oxygen levels. While our transcriptional analysis is not exhaustive, it is plausible that *tmpA* expression is constitutive in *St. sanguinis*. In *Ec. coli*, the gene encoding ZupT is constitutively transcribed at low levels (Grass et al., 2005).

In a recent study, Zhang et al. (2020) confirmed that in the human hZIP4, the M1 site is essential for metal transport and the M2 site facilitates optimal transport activity. Here we report that the modification of N173 to A or D in the predicted M2 site of TmpA resulted in the reduced function of the protein as a manganese transporter (Figure 9). This indicates TmpA cannot function efficiently without an asparagine in this position, despite the similar size and features of the aspartic acid. These results suggest that the charge of the side

chain at this position in TmpA likely contributes to either transport function, metal selectivity, or both. Future studies using cell-free metal uptake assays and structural analysis will be required to confirm our results.

The discovery that streptococci have different lineages of ZIP-family proteins suggests that these secondary transporters may be valuable to some species. However, this protein family is not essential in all streptococci as some species, such as the human pathogen *St. pyogenes* and the oral commensals *St. oralis* and *St. mitis*, have been evolutionarily successful without a ZIP-family protein. In some instances, MntH is encoded in the genomes of these species but *St. pyogenes* has only two sequenced strains that encode a MntH homolog, suggesting that the other strains either rely entirely on the primary ABC manganese transporter or encode an unidentified secondary transporter. At the other extreme, some streptococci encode all three transporters, similar to *St. sanguinis* VMC66 examined here. *St. mutans* is an example; however, the contribution of $ZupT_{Sm}$ to manganese transport has yet to be examined. A recent study found that it did not contribute significantly to zinc transport (Ganguly et al., 2021). Another study from the same group utilizing *St. mutans* manganese-transport mutants deleted for *sloC*, the *ssaB* homolog, and *mntH* found that the inactivation of MntH alone did not produce any obvious phenotype, whereas the Δ*sloC* and Δ*sloC* Δ*mntH* mutants were severely deficient under manganese-restricted conditions (Kajfasz et al., 2020). Further studies in both *St. mutans* and *St. sanguinis* would improve the understanding of the relative contribution of each of these proteins to growth, metal transport, and virulence and possibly reveal more about the origin of the distinct lineages.

In conclusion, we discovered that this ZIP-family protein, TmpA, contributes to manganese uptake and virulence in several strains of *St. sanguinis*, which is evident only after the deletion of the primary transporter. These results lay the foundation for future studies of manganese-transporter inhibitors for the prevention of IE, as both transporters could be targeted simultaneously to prevent the generation of spontaneous mutants that could subvert single-target treatment. Indeed, a study targeting BmtA to prevent *B. burgdorferi* virulence showed promising results (Wagh et al., 2015), although this study was completed before the crystallization of any ZIP-family protein. Additionally, inhibitors of SsaB orthologs have been under investigation, as they could potentially be used to treat other streptococcal diseases in addition to IE (Bajaj et al., 2015; Obaidullah et al., 2018). Furthermore, given that MntH does not significantly contribute to virulence but remains a functional manganese transporter at low pH (Puccio et al., 2022), its presence could lessen the effect of anti-SsaB drugs on the oral microbiota and may influence the selection of potential probiotic anti-caries streptococcal strains. Although future studies will be required, we hypothesize that anti-SsaB drugs could potentially remain effective at preventing IE without affecting growth or competitiveness of MntH-encoding streptococcal strains in the oral cavity. Taken together, these studies enhance our understanding of manganese transporters in *St. sanguinis* and the importance of manganese for the growth and virulence of this opportunistic pathogen.

4 | MATERIALS AND METHODS

4.1 | Bacterial strains and growth conditions

The *St. sanguinis* strains used in this study are listed in Table S1. Primers and plasmids used to generate the mutant strains are listed in Tables S2 and S3, respectively. *St. sanguinis* strains SK36, SK49, SK408, and SK678 are human isolates from Mogens Killian, Aarhus University, Denmark, characterized for virulence previously (Baker et al., 2019). VMC66 is a human blood isolate from Virginia Commonwealth University Medical Center Hospital (Baker et al., 2019; Kitten et al., 2012). All strains were grown in overnight cultures from single-use aliquots of cryopreserved cells, diluted 1000-fold in BHI media (Beckinson Dickinson). Mutant strains were incubated with the appropriate antibiotics: kanamycin (Kan; Sigma-Aldrich) at 500 μg/ml; tetracycline (Tet; Sigma-Aldrich) 5 μg/ml; erythromycin (Erm; Sigma-Aldrich) at 10 μg/ml; chloramphenicol (Cm; Fisher Scientific) at 5 μg/ml; and spectinomycin (Spc; Sigma-Aldrich) at 200 μg/ml. The cultures were then incubated at 37°C for 16–20 hr with the atmospheric condition set to 1% (1% O_2, 9.5% H_2, 9.5% CO_2 and 80% N_2), 6% (6% O_2, 7% H_2, 7% CO_2 and 80% N_2), or 12% (12% O_2, 4% H_2, 4% CO_2 and 80% N_2) oxygen using a programmable Anoxomat™ Mark II jar-filling system (AIG, Inc.). Overnight cultures of SK36 Δ*ssaACB* Δ*tmpA* mutants and the VMC66 Δ*ssaACB* Δ*mntH* strains were grown with 10 μM $MnSO_4$ added; the Δ*ssaACB* Δ*mntH* Δ*tmpA* strain typically required 15 μM $MnSO_4$.

Gene knockout mutant constructs were either generated previously (Xu et al., 2011) or by gene splicing by overlap extension (SOEing) PCR (Ho et al., 1989) where the gene(s) of interest were replaced with an antibiotic resistance gene or cassette. Transformations were performed using the protocol described previously (Paik et al., 2005). Briefly, an overnight culture of the parent strain was grown in Todd Hewitt (Beckinson Dickinson) broth with horse serum (Invitrogen), then diluted 200-fold and incubated at 37°C. Optical density (OD_{600}) of tube cultures was determined using a ThermoScientific BioMate 3S UV-VIS spectrophotometer. Knockout construct DNA (100 ng) and *St. sanguinis* competence stimulating peptide (70 ng) were added to the culture (OD_{600} ~0.07) and incubated at 37°C for 1.5 hr prior to selective plating on BHI agar plates with antibiotics at concentrations listed above. All plates were incubated for at least 24 hr at 37°C under anaerobic conditions in an Anoxomat jar with a palladium catalyst. The SK36 Δ*tmpA* strains were derived from SK36 WT and Δ*ssaACB*::*tetM* (JFP173), where *tmpA* was replaced with *aphA-3* using the SSX_1413 strain and primers from the SK36 knockout mutant library (Xu et al., 2011). The double mutant version was grown on BHI plates with 10 μM $MnSO_4$ added.

Markerless mutants were generated using a mutation system described previously (Cheng et al., 2018; Xie et al., 2011). Briefly,

the in-frame deletion cassette (IFDC) was amplified from the *St. sanguinis* IFDC2 strain and combined with flanking region from *tmpA* using gene SOEing. The parent strains were then transformed as described above, plating on BHI agar plates containing Erm. A gene SOEing product merging the two sides of *tmpA* with the desired nucleotide changes was then generated. This SOEing product was then used to transform the Erm^R colonies from the first transformation. Immediately prior to plating on agar plates containing 20 mM 4-chloro-phenylalanine (4-CP; Sigma-Aldrich), the cells were washed twice with phosphate buffered saline (PBS) to remove remaining media. The presence of the desired mutation was confirmed by Sanger sequencing. This method was also used to add the Strep-Tag II® sequence to each of the tagged mutants in its native genome location.

The complemented *tmpA* strain was generated using gene SOEing, which placed the *tmpA* gene under control of the Phyperspank promoter (Rhodes et al., 2014) and downstream of the Spc resistance cassette, *aad9*. This construct was inserted into the SSA_0169 gene on the chromosome (Turner et al., 2009). The SSA_0169::*tmpA*::ST (Loop III) strain was generated using same method, with the Strep-Tag II® sequence added between residues 109 and 110 of TmpA.

JFP36 is a previously generated marked WT strain (Turner et al., 2009) used for the in vivo experiments. All experiments with the SK36 version of the Δ*ssaACB* mutant used the Tet^R version (JFP173) with the following exceptions: the qRT-PCR experiment (Figure 5; Kan^R; JFP169) and one animal experiment (Figure 7b; Tet^R $Spec^R$; JFP234). Due to conflicts with antibiotic resistance, strain JFP234 was generated by amplifying the *aad9* gene and flanking DNA from the SSA_0169 locus in strain JFP56 (Turner et al., 2009) and introducing this product into JFP173, thus generating a Δ*ssaACB* mutant that is Spc^R to allow for selective plating in rabbit experiments. This strain was assessed for growth in serum and was indistinguishable from JFP173 (data not shown).

The Δ*ssaACB*, Δ*tmpA*, and Δ*mntH* mutants in strains other than SK36 were generated by using gene SOEing with primers specific to each strain background when identical primers were not possible. Since the SSA_0169 ectopic expression site from strain SK36 described above is not present in most other backgrounds examined, we previously generated a Spc^R VMC66 WT strain with the *aad9* gene inserted into a new, highly conserved ectopic expression site (Baker et al., 2019). Due to issues with overlapping antibiotic selection markers, another Δ*ssaACB* Δ*tmpA* mutant strain was generated for use exclusively in the rabbit virulence study that was Cm^R and Erm^R. Given that both Δ*ssaACB* Δ*tmpA* and Δ*ssaACB* Δ*mntH* were Cm^R, they were plated on Erm and Tet plates, respectively.

4.2 | Growth studies

Overnight BHI pre-cultures of each strain were made as described above. Tubes containing either 100% pooled rabbit serum (Gibco), BHI, or Chelex-treated (BioRad) BHI supplemented with 1 mM $CaCl_2$ and 1 mM $MgSO_4$ (cBHI) were pre-incubated at 37°C. The tubes were placed in Anoxomat jars set to either 1% O_2, 6% O_2, or 12% O_2 (12% O_2, 4.3% CO_2, 4.3% H_2) and incubated for 24 hr. Plating was used to enumerate colony-forming units (CFUs). To determine CFUs, samples were sonicated for 90 s using an ultrasonic homogenizer (Biologics, Inc) to disrupt chains prior to dilution in PBS and plated using an Eddy Jet 2 spiral plater (Neutec Group, Inc.).

For experiments in which metal was added, we employed the Puratronic™ line of metals (Alfa Aesar; $MnSO_4 \cdot H_2O$, $FeSO_4 \cdot H_2O$, and $ZnSO_4 \cdot H_2O$; 99.999% guaranteed purity). Each solution was made in Chelex-treated deionized water (cdH_2O) and added to the serum tubes immediately prior to inoculation. Fe^{2+} stocks were made fresh immediately prior to each experiment. For growth assessment of the complemented mutant, 1 mM IPTG (Fisher Scientific) was added to the serum tubes immediately prior to inoculation. For the Δ*adcC* mutant experiments, 1 μM TPEN (Sigma-Aldrich) and various concentrations of Zn^{2+} were added to the cBHI immediately prior to inoculation.

4.3 | Spot plating

Todd–Hewitt (BD) with 1% Yeast Extract (BD) agar plates were made with 100 μM Puratronic™ metals ($MnSO_4$, $FeSO_4$, or $ZnSO_4$). Overnight pre-cultures were grown as described above and then serially diluted in PBS. Cultures (10 μl) were spotted onto the plates aerobically, allowed to dry, and then incubated at 0% O_2 overnight before imaging.

4.4 | Metal analysis

Overnight BHI pre-cultures were grown as described above. Two tubes containing 38 ml BHI or cBHI were pre-incubated at 37°C for each experimental condition. The following day, 3 ml of the overnight culture was used to inoculate each 38-ml media tube. For cBHI experiments, pre-cultures were centrifuged and resuspended in warm cBHI prior to inoculation. Puratronic™ metals were prepared as described above and added immediately prior to inoculation. Inoculated cultures were placed back in the incubator. After several hours of growth, cells were harvested by centrifugation at 3,740 × *g* for 10 min at 4°C. The supernatant was decanted and the cell pellet was washed twice with cold cPBS (PBS treated with Chelex-100 resin for 2 hr, then filter sterilized and supplemented with EDTA [Invitrogen] to 1 mM). The pellet was then divided for subsequent acid digestion or protein concentration determination. Trace metal grade (TMG) nitric acid (15%; Fisher Chemical) was added to one portion of the pellet. The pellet was digested using an Anton Paar microwave digestion system and a modified Organic B protocol: 120°C for 10 min, 180°C for 20 min, with the maximum temperature set to 180°C. The digested samples were then diluted 3-fold with cdH_2O. Metal concentrations were determined using an Agilent 5110 inductively coupled plasma-optical emission

spectrometer. Concentrations were determined by comparison with a standard curve created with a 10 μg/ml multi-element standard (CMS-5; Inorganic Ventures) diluted in 5% TMG nitric acid. Pb (Inorganic Ventures) was used as an internal standard (10 μg/ml). The other portion of the pellet was resuspended in PBS and mechanically lysed using a FastPrep-24 instrument with Lysing Matrix B tubes (MP Biomedicals) as described previously (Rhodes et al., 2014). Insoluble material was removed by centrifugation. Protein concentrations were determined using a bicinchoninic acid (BCA) Protein Assay Kit (Pierce) as recommended by the manufacturer, with bovine serum albumin as the standard. Absorbance was measured in a black-walled, flat-bottom 96-well plate (Greiner) using a microplate reader (BioTek).

4.5 | Quantitative real-time polymerase chain reaction

Overnight cultures of SK36 WT and Δ*ssaACB* (JFP169) strains were grown as described above then subjected to one of three protocols. In the first, they were then diluted 10-fold into BHI and incubated aerobically (~21% O_2). Once cells reached mid-log phase (OD_{600} ~0.6), 6 ml of culture was separated into tubes for each condition and 100 μM Puratronic™ metal ($MnSO_4$, $ZnSO_4$, or $FeSO_4$) or EDTA (Invitrogen) was added. A culture tube with no additives was included as the control. Tubes were incubated aerobically without a jar at 37°C for 15 min. To collect cells, the tubes were swirled in a dry ice/ethanol bath for 30 s prior to centrifugation for 10 min at 3,740 × *g* at 4°C. The supernatant was discarded and the samples were stored at −80°C. In the second protocol, overnight cultures of SK36 and JFP169 were grown in an anaerobic chamber (Coy Laboratory Products). Cells were then diluted 10-fold into BHI pre-incubated anaerobically at 37°C. At mid-log phase, cultures were separated and 6 ml of cells were collected immediately and 6 ml of cells were incubated aerobically (~21% O_2) for 15 min. Cells were collected as above. In the third protocol, cells were diluted 10-fold into BHI pre-incubated in 6% O_2. Metals were added to each tube just prior to inoculation and incubation was continued for ~2.5 hr (to OD_{600} ~0.6) and then cells were harvested for RNA isolation as above. RNA isolation and on-column DNase treatment were completed using the RNeasy Mini Kit and RNase-Free DNase Kit, respectively (Qiagen). RNA was eluted in 50 μl RNase-Free water (Qiagen). A second DNase treatment was then performed on the samples (Invitrogen). Total RNA was quantified and purity was assessed using a Nanodrop 2000 Spectrophotometer (ThermoScientific). Libraries of cDNA were created using SensiFAST cDNA Synthesis Kit (Bioline). Control reactions without reverse transcriptase were conducted to confirm the absence of contaminating DNA in all samples. Quantitative real-time polymerase chain reaction (qRT-PCR) was performed using SYBR Green Supermix (Applied Biosystems) on an Applied Biosystems 7500 Fast Real-Time PCR System using the primers listed in Table S4. Relative gene expression was analyzed using the $2^{-\Delta\Delta CT}$ method (Livak & Schmittgen, 2001) with *gapA* serving as the internal control (Rodriguez et al., 2011).

4.6 | In vivo virulence assays

Virulence assays were performed using a rabbit model of infective endocarditis (Paik et al., 2005). Specific pathogen-free New Zealand white rabbits weighing 2–4 kg were purchased from RSI Biotechnology and Charles River Laboratories. We allowed them to acclimate to the vivarium at least 7 days prior to inoculation. The rabbits were anesthetized and a 19-gauge catheter (BD Bioscience) was inserted through the right internal carotid artery past the aortic valve to cause minor damage. The catheter was trimmed, sutured in place, and remained in the artery for the entire experiment. The incision was closed with staples. *St. sanguinis* experimental strains were grown overnight in BHI at 1% or 6% O_2, diluted 10-fold into fresh BHI, incubated for 3 hr, sonicated, washed, and resuspended in PBS. The inoculum was further diluted in PBS to obtain desired cell concentrations and 0.5 ml of combined culture was inoculated via intravenous injection into an ear vein on the second day after surgery. For studies only assessing the virulence of single manganese transport systems, each strain was inoculated at ~1×10^7 CFU/ml. For studies assessing combination mutants of multiple systems, WT was inoculated at ~5×10^6 CFU/ml and each Δ*ssaACB* derivative strain was inoculated at ~1×10^8 CFU/ml. Spare inoculum culture was plated on BHI agar with appropriate antibiotics to confirm bacterial counts. At 20 hr post-inoculation, rabbits were euthanized by intravenous injection of Euthasol (Virbac AH). Following removal of the heart, catheter placement was verified and vegetations were removed. Vegetations were homogenized with PBS, sonicated, diluted, and plated on BHI agar with appropriate antibiotics as above. The results were reported as recovered CFU per rabbit for each strain and normalized to inocula ratios. All animal procedures were approved by Virginia Commonwealth University Institutional Animal Care and Use Committee and complied with applicable federal and institutional guidelines.

4.7 | Protein modeling and depiction

Alignment of TmpA, BmtA, and ZIPB was performed with Clustal W in Geneious 11.1 (geneious.com). TMDs were based on the α-helices of the crystal structure of ZIPB (5TSA). Depiction of TmpA in 2D was generated in Protter (Omasits et al., 2014) and modified to match the TMDs determined in the alignment. Protein models were built in SYBYL-X 2.0. The alignment of TmpA TMD III was adjusted to best fit ZIPB TMD III due to the differences in length, although a "bridge" still is present where a helix should be. The N-terminus and loop between TMDs III and IV were removed from the alignment for the model since they were not present in the crystal structure due to inherent disorder.

Water molecules and metal ions were removed from the ZIPB protein (PDB: 5TSA) and hydrogen atoms were retained. One hundred models were built, minimized with hydrogens over 10,000 iterations with a gradient of 0.5 and a Gastieger-Huckel charge. One model was chosen for further analysis with an RMSD of 1.783. Residue N173 was replaced with D and the model was again minimized as described above.

Positions within a cellular membrane were predicted using OPM (https://opm.phar.umich.edu/) and visualized in JMol 3.0 using FirstGlance (http://jmol.sourceforge.net/).

4.8 | Evolutionary analysis

Sequences of *St. sanguinis* SK36 TmpA and SsaB and *St. mutans* UA159 TmpA were used as queries for BLASTP searches of the Non-redundant protein or Refseq Select proteins database and the top hits were selected. For each species selected, only one sequence was used for the phylogenetic analysis. The evolutionary history was inferred using the Neighbor-Joining method (Saitou & Nei, 1987) with a gap opening penalty of 3.0 and a gap extension penalty of 1.8 for the multiple alignment stage (Hall, 2008). The evolutionary distances were computed using the Poisson correction method (Zuckerkandl & Pauling, 1965) and are in the units of number of amino acid substitutions per site. All ambiguous positions were removed for each sequence pair. Evolutionary analyses were conducted in MEGAX (Kumar et al., 2018). 16S rRNA groups of streptococci, with the exception of *St. ratti*, were labeled based on Nobbs et al. (2009).

4.9 | Data analysis and presentation

Statistical tests were performed in GraphPad Prism (graphpad.com) and significance was determined by *t*-test or analysis of variance (ANOVA) as indicated in the figure legends. Tests were paired only if matching was effective. *p*-values ≤ .05 were considered significant. Graphs and figures were constructed using GraphPad Prism (graphpad.com) or Biorender (Biorender.com).

ACKNOWLEDGMENTS

We thank Ping Xu (VCU Philips Institute) for use of his strains and Jens Kreth and Nyssa Cullin (Oregon Health & Science University) for providing the IFDC *St. sanguinis* strain and corresponding protocol. We would like to thank Shannon Green, Nicai Zollar, and Rachel Korba (VCU Philips Institute) for their assistance with animal experiments. We are grateful for the advice and technical support of Joseph Turner (VCU Department of Chemistry) and the protein modeling assistance provided by Glenn Kellogg and Claudio Catalano (VCU Department of Medicinal Chemistry). We appreciate the membrane protein technical advice of David Eide (University of Wisconsin-Madison), Nick Noinaj (Purdue University), Jeannine Brady (University of Florida), Brian Kloss (Center on Membrane Protein Production and Analysis), and Sara Palmer. We would also like to sincerely thank Ross Belvin (VCU Philips Institute) for his advice and review of the manuscript. Finally, we thank the anonymous reviewers for their helpful suggestions.

CONFLICT OF INTEREST

Authors have no conflicts to disclose.

AUTHOR CONTRIBUTIONS

TP, KK, and SSA performed the experiments. TP and TK wrote the manuscript. All authors reviewed and approved the final version of the manuscript.

ETHICS APPROVAL

The Virginia Commonwealth University Institutional Animal Care and Use Committee approved all animal procedures (IACUC Protocol #AM10030), ensuring compliance with PHS Policy on Humane Care and Use of Laboratory Animals, The Guide for the Care and Use of Laboratory Animals, and all other applicable regulations.

DATA AVAILABILITY STATEMENT

The data that support the findings of this study are available from the corresponding author upon reasonable request (Puccio et al., 2021).

ORCID

Tanya Puccio https://orcid.org/0000-0002-0223-4885
Seon-Sook An https://orcid.org/0000-0002-7481-9612
Todd Kitten https://orcid.org/0000-0001-6097-7583

REFERENCES

Altschul, S.F., Gish, W., Miller, W., Myers, E.W. & Lipman, D.J. (1990) Basic local alignment search tool. *Journal of Molecular Biology*, *215*(3), 403–410.

Anjem, A. & Imlay, J.A. (2012) Mononuclear iron enzymes are primary targets of hydrogen peroxide stress. *Journal of Biological Chemistry*, *287*, 15544–15556.

Atkuri, K.R., Herzenberg, L.A., Niemi, A.-K., Cowan, T. & Herzenberg, L.A. (2007) Importance of culturing primary lymphocytes at physiological oxygen levels. *Proceedings of the National Academy of Sciences of the United States of America*, *104*, 4547–4552. https://doi.org/10.1073/pnas.0611732104

Aydemir, T.B., Kim, M.H., Kim, J., Colon-Perez, L.M., Banan, G., Mareci, T.H. et al. (2017) Metal transporter ZIP14 (SLC39A14) deletion in mice increases manganese deposition and produces neurotoxic signatures and diminished motor activity. *Journal of Neuroscience*, *37*, 5996–6006.

Bajaj, M., Mamidyala, S.K., Zuegg, J., Begg, S.L., Ween, M.P., Luo, Z. et al. (2015) Discovery of novel pneumococcal surface antigen A (PsaA) inhibitors using a fragment-based drug design approach. *ACS Chemical Biology*, *10*, 1511–1520. https://doi.org/10.1021/cb501032x

Baker, S.P., Nulton, T.J. & Kitten, T. (2019) Genomic, phenotypic, and virulence analysis of *Streptococcus sanguinis* oral and infective-endocarditis isolates. *Infection and Immunity*, *87*, e00703-18.

Bashore, T.M., Cabell, C. & Fowler, V. Jr (2006) Update on infective endocarditis. *Current Problems in Cardiology*, *31*(4), 274–352. https://doi.org/10.1016/j.cpcardiol.2005.12.001

Bozzi, A.T., Bane, L.B., Weihofen, W.A., McCabe, A.L., Singharoy, A., Chipot, C.J. et al. (2016) Conserved methionine dictates substrate preference in Nramp-family divalent metal transporters. *Proceedings of the National Academy of Sciences of the United States of America*, *113*, 10310–10315. https://doi.org/10.1073/pnas.1607734113

Cheng, X., Redanz, S., Cullin, N., Zhou, X., Xu, X., Joshi, V. et al. (2018) Plasticity of the pyruvate node modulates hydrogen peroxide production and acid tolerance in multiple oral streptococci. *Applied and Environmental Microbiology*, *84*, e01697-17. https://doi.org/10.1128/AEM.01697-17

Colomer-Winter, C., Flores-Mireles, A.L., Baker, S.P., Frank, K.L., Lynch, A.J.L., Hultgren, S.J. et al. (2018) Manganese acquisition is essential for virulence of *Enterococcus faecalis*. *PLoS Pathogens*, *14*, e1007102. https://doi.org/10.1371/journal.ppat.1007102

Counago, R.M., Ween, M.P., Begg, S.L., Bajaj, M., Zuegg, J., O'Mara, M.L. et al. (2014) Imperfect coordination chemistry facilitates metal ion release in the Psa permease. *Nature Chemical Biology*, *10*, 35–41.

Crump, K.E., Bainbridge, B., Brusko, S., Turner, L.S., Ge, X., Stone, V. et al. (2014) The relationship of the lipoprotein SsaB, manganese and superoxide dismutase in *Streptococcus sanguinis* virulence for endocarditis. *Molecular Microbiology*, *92*, 1243–1259.

Das, S., Kanamoto, T., Ge, X., Xu, P., Unoki, T., Munro, C.L. et al. (2009) Contribution of lipoproteins and lipoprotein processing to endocarditis virulence in *Streptococcus sanguinis*. *Journal of Bacteriology*, *191*, 4166–4179.

Dayer, M. & Thornhill, M. (2018) Is antibiotic prophylaxis to prevent infective endocarditis worthwhile?. *Journal of Infection and Chemotherapy*, *24*(1), 18–24. http://dx.doi.org/10.1016/j.jiac.2017.10.006

Dempski, R.E. (2012) The cation selectivity of the ZIP transporters. *Current Topics in Membranes*, *69*, 221–245.

Di Filippo, S., Delahaye, F., Semiond, B., Celard, M., Henaine, R., Ninet, J. et al. (2006) Current patterns of infective endocarditis in congenital heart disease. *Heart*, *92*, 1490–1495. https://doi.org/10.1136/hrt.2005.085332

Diaz-Ochoa, V.E., Jellbauer, S., Klaus, S. & Raffatellu, M. (2014) Transition metal ions at the crossroads of mucosal immunity and microbial pathogenesis. *Frontiers in Cellular and Infection Microbiology*, *4*, 2. https://doi.org/10.3389/fcimb.2014.00002

Dintilhac, A., Alloing, G., Granadel, C. & Claverys, J.-P. (1997) Competence and virulence of *Streptococcus pneumoniae*: Adc and PsaA mutants exhibit a requirement for Zn and Mn resulting from inactivation of putative ABC metal permeases. *Molecular Microbiology*, *25*, 727–739.

Dodds, D.R. (2017) Antibiotic resistance: a current epilogue. *Biochemical Pharmacology*, *134*, 139–146.

Ehrnstorfer, I.A., Geertsma, E.R., Pardon, E., Steyaert, J. & Dutzler, R. (2014) Crystal structure of a SLC11 (NRAMP) transporter reveals the basis for transition-metal ion transport. *Nature Structural and Molecular Biology*, *21*, 990–996.

Eide, D.J. (2004) The SLC39 family of metal ion transporters. *Pflugers Archiv. European Journal of Physiology*, *447*, 796–800. https://doi.org/10.1007/s00424-003-1074-3

Eide, D.J. (2012) An "inordinate fondness for transporters" explained? *Science Signalling*, *5*, pe5. https://doi.org/10.1126/scisignal.2002837

Eide, D., Broderius, M., Fett, J. & Guerinot, M.L. (1996) A novel iron-regulated metal transporter from plants identified by functional expression in yeast. *Proceedings of the National Academy of Sciences of the United States of America*, *93*, 5624–5628. https://doi.org/10.1073/pnas.93.11.5624

Eijkelkamp, B.A., McDevitt, C.A. & Kitten, T. (2015) Manganese uptake and streptococcal virulence. *BioMetals*, *28*, 491–508. https://doi.org/10.1007/s10534-015-9826-z

Fujishiro, H. & Himeno, S. (2019) New insights into the roles of ZIP8, a cadmium and manganese transporter, and its relation to human diseases. *Biological and Pharmaceutical Bulletin*, *42*, 1076–1082.

Gaither, L.A. & Eide, D. (2001) Eukaryotic zinc transporters and their regulation. *BioMetals*, *14*, 251–270.

Ganguly, T., Peterson, A.M., Kajfasz, J.K., Abranches, J. & Lemos, J.A. (2021) Zinc import mediated by AdcABC is critical for colonization of the dental biofilm by *Streptococcus mutans* in an animal model. *Molecular Oral Microbiology*, *36*, 214–224.

Grass, G., Franke, S., Taudte, N., Nies, D.H., Kucharski, L.M., Maguire, M.E. et al. (2005) The metal permease ZupT from *Escherichia coli* is a transporter with a broad substrate spectrum. *Journal of Bacteriology*, *187*, 1604–1611.

Grass, G., Wong, M.D., Rosen, B.P., Smith, R.L. & Rensing, C. (2002) ZupT is a Zn(II) uptake system in *Escherichia coli*. *Journal of Bacteriology*, *184*, 864–866.

Guerinot, M.L. (2000) The ZIP family of metal transporters. *Biochimica Et Biophysica Acta (BBA) - Biomembranes*, *1465*, 190–198. https://doi.org/10.1016/S0005-2736(00)00138-3

Hall, B.G. (2008) *Phylogenetic trees made easy*. Sinauer Associates.

Ho, S.N., Hunt, H.D., Horton, R.M., Pullen, J.K. & Pease, L.R. (1989) Site-directed mutagenesis by overlap extension using the polymerase chain reaction. *Gene*, *77*, 51–59. https://doi.org/10.1016/0378-1119(89)90358-2

Jamil, M., Sultan, I., Gleason, T.G., Navid, F., Fallert, M.A., Suffoletto, M.S. et al. (2019) Infective endocarditis: trends, surgical outcomes, and controversies. *Journal of Thoracic Disease*, *11*, 4875–4885. https://doi.org/10.21037/jtd.2019.10.45

Jeong, J. & Eide, D.J. (2013) The SLC39 family of zinc transporters. *Molecular Aspects of Medicine*, *34*, 612–619. https://doi.org/10.1016/j.mam.2012.05.011

Johnston, J.W., Briles, D.E., Myers, L.E. & Hollingshead, S.K. (2006) Mn^{2+}-dependent regulation of multiple genes in *Streptococcus pneumoniae* through PsaR and the resultant impact on virulence. *Infection and Immunity*, *74*, 1171–1180.

Juttukonda, L.J. & Skaar, E.P. (2015) Manganese homeostasis and utilization in pathogenic bacteria. *Molecular Microbiology*, *97*, 216–228.

Kajfasz, J.K., Katrak, C., Ganguly, T., Vargas, J., Wright, L., Peters, Z.T. et al. (2020) Manganese uptake, mediated by SloABC and MntH, is essential for the fitness of *Streptococcus mutans*. *mSphere*, *5*, e00764-19. https://doi.org/10.1128/mSphere.00764-19

Kehl-Fie, T.E., Zhang, Y., Moore, J.L., Farrand, A.J., Hood, M.I., Rathi, S. et al. (2013) MntABC and MntH contribute to systemic *Staphylococcus aureus* infection by competing with calprotectin for nutrient manganese. *Infection and Immunity*, *81*, 3395–3405.

Kehres, D.G. & Maguire, M.E. (2003) Emerging themes in manganese transport, biochemistry and pathogenesis in bacteria. *FEMS Microbiology Reviews*, *27*, 263–290.

Kelliher, J.L. & Kehl-Fie, T.E. (2016) Competition for manganese at the host-pathogen interface. *Progress in molecular biology and translational science*, *142*, 1–25.

Kitten, T., Munro, C.L., Zollar, N.Q., Lee, S.P. & Patel, R.D. (2012) Oral streptococcal bacteremia in hospitalized patients: taxonomic identification and clinical characterization. *Journal of Clinical Microbiology*, *50*, 1039–1042. https://doi.org/10.1128/JCM.06438-11

Kreth, J., Merritt, J., Shi, W. & Qi, F. (2005) Competition and coexistence between *Streptococcus mutans* and *Streptococcus sanguinis* in the dental biofilm. *Journal of Bacteriology*, *187*, 7193–7203.

Kumar, S., Stecher, G., Li, M., Knyaz, C. & Tamura, K. (2018) MEGA X: molecular evolutionary genetics analysis across computing platforms. *Molecular Biology and Evolution*, *35*, 1547–1549. https://doi.org/10.1093/molbev/msy096

Lin, W., Chai, J., Love, J. & Fu, D. (2010) Selective electrodiffusion of zinc ions in a Zrt-, Irt-like protein, ZIPB. *Journal of Biological Chemistry*, *285*, 39013–39020.

Livak, K.J. & Schmittgen, T.D. (2001) Analysis of relative gene expression data using real-time quantitative PCR and the $2^{(-\Delta\Delta CT)}$ method. *Methods*, *25*, 402–408.

Ly, R., Compain, F., Gaye, B., Pontnau, F., Bouchard, M. & Mainardi, J.L. (2021) Predictive factors of death associated with infective endocarditis in adult patients with congenital heart disease. *European Heart Journal. Acute Cardiovascular Care*, *10*(3), 320–328. http://dx.doi.org/10.1177/2048872620901394

Martin, J.E. & Giedroc, D.P. (2016) Functional determinants of metal ion transport and selectivity in paralogous cation diffusion facilitator transporters CzcD and MntE in *Streptococcus pneumoniae*. *Journal of Bacteriology*, *198*, 1066–1076. https://doi.org/10.1128/JB.00975-15

Morrision, K.L. & Weiss, G.A. (2001) Combinatorial alanine-scanning. *Current Opinion in Chemical Biology*, *5*, 302–307.

Murgas, C.J., Green, S.P., Forney, A.K., Korba, R.M., An, S.S., Kitten, T. et al. (2020) Intracellular metal speciation in *Streptococcus sanguinis* establishes SsaACB as critical for redox maintenance. *ACS Infectious Diseases*, *6*, 1906–1921.

Nevo, Y. & Nelson, N. (2006) The NRAMP family of metal-ion transporters. *Biochimica et Biophysica Acta (BBA) - Molecular Cell Research*, *1763*(7), 609–620. http://dx.doi.org/10.1016/j.bbamcr.2006.05.007

Nobbs A. H., Lamont R. J. & Jenkinson H. F. (2009) Streptococcus adherence and colonization. *Microbiology and Molecular Biology Reviews*, *73*(3), 407–450. http://dx.doi.org/10.1128/mmbr.00014-09

Obaidullah, A.J., Ahmed, M.H., Kitten, T. & Kellogg, G.E. (2018) Inhibiting pneumococcal surface antigen A (PsaA) with small molecules discovered through virtual screening: steps toward validating a potential target for *Streptococcus pneumoniae*. *Chemistry and Biodiversity*, *15*, e1800234.

Omasits, U., Ahrens, C.H., Muller, S. & Wollscheid, B. (2014) Protter: interactive protein feature visualization and integration with experimental proteomic data. *Bioinformatics*, *30*, 884–886. https://doi.org/10.1093/bioinformatics/btt607

Ouyang, Z., He, M., Oman, T., Yang, X.F. & Norgard, M.V. (2009) A manganese transporter, BB0219 (BmtA), is required for virulence by the Lyme disease spirochete, *Borrelia burgdorferi*. *Proceedings of the National Academy of Sciences of the United States of America*, *106*, 3449–3454. https://doi.org/10.1073/pnas.0812999106

Paik, S., Senty, L., Das, S., Noe, J.C., Munro, C.L. & Kitten, T. (2005) Identification of virulence determinants for endocarditis in *Streptococcus sanguinis* by signature-tagged mutagenesis. *Infection and Immunity*, *73*, 6064–6074.

Park, J.H., Hogrebe, M., Gruneberg, M., DuChesne, I., von der Heiden, A.L., Reunert, J. et al. (2015) SLC39A8 deficiency: a disorder of manganese transport and glycosylation. *American Journal of Human Genetics*, *97*, 894–903.

Puccio, T. (2020) The role of manganese in *Streptococcus sanguinis*. Virginia Commonwealth University Dissertation, 1–235.

Puccio, T., An, S.-S., Schultz, A.C., Lizarraga, C.A., Bryant, A.S., Culp, D.J. et al. (2022) Manganese transport by Streptococcus sanguinis in acidic conditions and its impact on growth in vitro and in vivo. *Molecular Microbiology*, *117*, 375–393. https://doi.org/10.1111/mmi.14854

Puccio, T., Kunka, K.S., An, S.-S. & Kitten, T. (2021) [dataset] Contribution of a ZIP-family protein to manganese uptake and infective endocarditis virulence in Streptococcus sanguinis. In: Data available upon request.

Puccio, T., Kunka, K.S., Zhu, B., Xu, P. & Kitten, T. (2020) Manganese depletion leads to multisystem changes in the transcriptome of the opportunistic pathogen *Streptococcus sanguinis*. *Frontiers in Microbiology*, *11*, 592615. https://doi.org/10.3389/fmicb.2020.592615

Quan, T.P., Muller-Pebody, B., Fawcett, N., Young, B.C., Minaji, M., Sandoe, J. et al. (2020) Investigation of the impact of the NICE guidelines regarding antibiotic prophylaxis during invasive dental procedures on the incidence of infective endocarditis in England: an electronic health records study. *BMC Medicine*, *18*, 84. https://doi.org/10.1186/s12916-020-01531-y

Raimunda, D., Gonzalez-Guerrero, M., Leeber, B.W. 3rd & Arguello, J.M. (2011) The transport mechanism of bacterial Cu^{+}-ATPases: distinct efflux rates adapted to different function. *BioMetals*, *24*, 467–475. https://doi.org/10.1007/s10534-010-9404-3

Ramsey, M.E., Hyde, J.A., Medina-Perez, D.N., Lin, T., Gao, L., Lundt, M.E. et al. (2017) A high-throughput genetic screen identifies previously uncharacterized *Borrelia burgdorferi* genes important for resistance against reactive oxygen and nitrogen species. *PLoS Pathogens*, *13*, e1006225. https://doi.org/10.1371/journal.ppat.1006225

Ravenhall, M., Škunca, N., Lassalle, F. & Dessimoz, C. (2015) Inferring horizontal gene transfer. *PLoS Computational Biology*, *11*, e1004095. https://doi.org/10.1371/journal.pcbi.1004095

Rhodes, D.V., Crump, K.E., Makhlynets, O., Snyder, M., Ge, X., Xu, P. et al. (2014) Genetic characterization and role in virulence of the ribonucleotide reductases of *Streptococcus sanguinis*. *Journal of Biological Chemistry*, *289*, 6273–6287.

Richards, V.P., Palmer, S.R., Pavinski Bitar, P.D., Qin, X., Weinstock, G.M., Highlander, S.K. et al. (2014) Phylogenomics and the dynamic genome evolution of the genus *Streptococcus*. *Genome Biology and Evolution*, *6*, 741–753. https://doi.org/10.1093/gbe/evu048

Rodriguez, A.M., Callahan, J.E., Fawcett, P., Ge, X., Xu, P. & Kitten, T. (2011) Physiological and molecular characterization of genetic competence in *Streptococcus sanguinis*. *Molecular Oral Microbiology*, *26*, 99–116. https://doi.org/10.1111/j.2041-1014.2011.00606.x

Saitou, N. & Nei, M. (1987) The neighbor-joining method: a new method for reconstructing phylogenetic trees. *Molecular Biology and Evolution*, *4*, 406–425.

Scheiber, I.F., Wu, Y., Morgan, S.E. & Zhao, N. (2019) The intestinal metal transporter ZIP14 maintains systemic manganese homeostasis. *Journal of Biological Chemistry*, *294*, 9147–9160.

Shabayek, S., Bauer, R., Mauerer, S., Mizaikoff, B. & Spellerberg, B. (2016) A streptococcal NRAMP homologue is crucial for the survival of *Streptococcus agalactiae* under low pH conditions. *Molecular Microbiology*, *100*, 589–606.

Taudte, N. & Grass, G. (2010) Point mutations change specificity and kinetics of metal uptake by ZupT from *Escherichia coli*. *BioMetals*, *23*, 643–656. https://doi.org/10.1007/s10534-010-9319-z

Thornhill, M.H., Gibson, T.B., Cutler, E., Dayer, M.J., Chu, V.H., Lockhart, P.B. et al. (2018) Antibiotic prophylaxis and incidence of endocarditis before and after the 2007 AHA recommendations. *Journal of the American College of Cardiology*, *72*, 2443–2454.

Turner, L.S., Das, S., Kanamoto, T., Munro, C.L. & Kitten, T. (2009) Development of genetic tools for *in vivo* virulence analysis of *Streptococcus sanguinis*. *Microbiology*, *155*, 2573–2582. https://doi.org/10.1099/mic.0.024513-0

Wagh, D., Pothineni, V.R., Inayathullah, M., Liu, S., Kim, K.-M. & Rajadas, J. (2015) Borreliacidal activity of Borrelia metal transporter A (BmtA) binding small molecules by manganese transport inhibition. *Drug Design, Development and Therapy*, *2015*(9), 805–816. http://dx.doi.org/10.2147/dddt.s77063

Waters, L.S. (2020) Bacterial manganese sensing and homeostasis. *Current Opinion in Chemical Biology*, *55*, 96–102.

Wilson, W.R., Gewitz, M., Lockhart, P.B., Bolger, A.F., DeSimone, D.C., Kazi, D.S. et al. (2021) Prevention of viridans group streptococcal infective endocarditis: a scientific statement from the American Heart Association. *Circulation*, *143*, e963–e978. https://doi.org/10.1161/CIR.0000000000000969

Wilson, W., Taubert, K.A., Gewitz, M., Lockhart, P.B., Baddour, L.M., Levison, M. et al. (2007) Prevention of infective endocarditis: guidelines from the American Heart Association. *Circulation*, *116*, 1736–1754. https://doi.org/10.1161/CIRCULATIONAHA.106.183095

Wray, D., Ruiz, F., Richey, R. & Stokes, T. (2008) Prophylaxis against infective endocarditis for dental procedures – summary of the NICE

guideline. *British Dental Journal*, *204*(10), 555–557. http://dx.doi.org/10.1038/sj.bdj.2008.404

Xie, Z., Okinaga, T., Qi, F., Zhang, Z. & Merritt, J. (2011) Cloning-independent and counterselectable markerless mutagenesis system in *Streptococcus mutans*. *Applied and Environment Microbiology*, *77*, 8025–8033.

Xu, P., Alves, J.M., Kitten, T., Brown, A., Chen, Z., Ozaki, L.S. et al. (2007) Genome of the opportunistic pathogen *Streptococcus sanguinis*. *Journal of Bacteriology*, *189*, 3166–3175.

Xu, P., Ge, X., Chen, L., Wang, X., Dou, Y., Xu, J.Z. et al. (2011) Genome-wide essential gene identification in *Streptococcus sanguinis*. *Scientific Reports*, *1*, 1–9. https://doi.org/10.1038/srep00125

Yu, Y., Wu, A., Zhang, Z., Yan, G., Zhang, F., Zhang, L. et al. (2013) Characterization of the GufA subfamily member SLC39A11/Zip11 as a zinc transporter. *Journal of Nutritional Biochemistry*, *24*, 1697–1708. https://doi.org/10.1016/j.jnutbio.2013.02.010

Zackular, J.P., Knippel, R.J., Lopez, C.A., Beavers, W.N., Maxwell, C.N., Chazin, W.J. et al. (2020) ZupT facilitates *Clostridioides difficile* resistance to host-mediated nutritional immunity. *mSphere*, *5*, e00061-20. https://doi.org/10.1128/mSphere.00061-20

Zhang, T., Kuliyev, E., Sui, D. & Hu, J. (2019) The histidine-rich loop in the extracellular domain of ZIP4 binds zinc and plays a role in zinc transport. *The Biochemical Journal*, *476*, 1791–1803.

Zhang, T., Liu, J., Fellner, M., Zhang, C., Sui, D. & Hu, J. (2017) Crystal structures of a ZIP zinc transporter reveal a binuclear metal center in the transport pathway. *Science Advances*, *3*, e1700344. https://doi.org/10.1126/sciadv.1700344

Zhang, T., Sui, D., Zhang, C., Cole, L. & Hu, J. (2020) Asymmetric functions of a binuclear metal center within the transport pathway of a human zinc transporter ZIP4. *The FASEB Journal*, *34*, 237–247. https://doi.org/10.1096/fj.201902043R

Zhao, H. & Eide, D. (1996a) The yeast ZRT1 gene encodes the zinc transporter protein of a high-affinity uptake system induced by zinc limitation. *Proceedings of the National Academy of Sciences of the United States of America*, *93*, 2454–2458. https://doi.org/10.1073/pnas.93.6.2454

Zhao, H. & Eide, D. (1996) The ZRT2 Gene Encodes the Low Affinity Zinc Transporter in Saccharomyces cerevisiae. *Journal of Biological Chemistry*, *271*(38), 23203–23210. http://dx.doi.org/10.1074/jbc.271.38.23203

Zuckerkandl, E. & Pauling, L. (1965) Evolutionary divergence and convergence in proteins. In: H.J., Vogel & V. Bryson (Eds.) *Evolving genes and proteins*. Academic Press. pp. 97–166.

SUPPORTING INFORMATION

Additional supporting information may be found in the online version of the article at the publisher's website.

How to cite this article: Puccio, T., Kunka, K.S., An, S.-S. & Kitten, T. (2022) Contribution of a ZIP-family protein to manganese uptake and infective endocarditis virulence in *Streptococcus sanguinis*. *Molecular Microbiology*, 117, 353–374. https://doi.org/10.1111/mmi.14853